Plant Physiology Preview. Published on September 3, 2015, as DOI:10.1104/pp.15.01122

Running Title:

Functional redundancy of Trx *f* and NTRC systems

Corresponding author:

Peter Geigenberger
Ludwig-Maximilians-Universität München
Department Biologie I
Grosshaderner Str. 2-4
82152 Martinsried, Germany
Tel: (49) 89 2180 74710
Mail: geigenberger@bio.lmu.de

Research Area:

Biochemistry and Metabolism

Thioredoxin *f*1 and NADPH-dependent thioredoxin reductase C have overlapping functions in regulating photosynthetic metabolism and plant growth in response to varying light conditions

Ina Thormählen, Tobias Meitzel, Julia Groysman, Alexandra Bianca Öchsner, Edda von Roepenack-Lahaye, Belén Naranjo, Francisco J. Cejudo and Peter Geigenberger*[1]

Ludwig-Maximilians-Universität München, Department Biologie I, Grosshaderner Str. 2-4, 82152 Martinsried, Germany (I.T., J.G., A.B.Ö., E.v.R.-L., P.G.)
Leibniz-Institut für Pflanzengenetik und Kulturpflanzenforschung, Corrensstr. 3, 06466 Gatersleben, Germany (T.M.)
Instituto de Bioquímica Vegetal y Fotosíntesis, University of Seville and CSIC, Avda Américo Vespucio 49, 41092-Sevilla, Spain (B.N., F.J.C.)

One Sentence Summary:
There is a previously unrecognized comunication between light and NADPH dependent thiol-redox systems in regulating photosynthetic metabolism and growth in response to varying light conditions.

Footnotes:
[1]This work was supported by funding from the Deutsche Forschungsgemeinschaft (grants Ge 878/5-2, Ge 878/8-1 and INST 86/1254-1 to P.G.). Work in F.J.C.'s lab was supported by grant BIO2013-43556-P of the Spanish Ministry of Economy and Competitivity. Scientific exchange between Munich and Seville was supported by funds of a German-Spanish interaction program (grants DAAD-50750315 to P.G and AIB2010DE-0029 to F. J.C.).
*Address correspondence to geigenberger@bio.lmu.de.

The author responsible for distribution of materials integral to the findings presented in this article in accordance with the policy described in the Instructions for Authors (www.plantcell.org) is: Peter Geigenberger (geigenberger@bio.lmu.de).

ABSTRACT

Two different thiol-redox-systems exist in plant chloroplasts, the ferredoxin-thioredoxin system, which depends of ferredoxin reduced by the photosynthetic electron-transport chain and, thus, of light, and the NADPH-dependent thioredoxin reductase C (NTRC) system, which relies on NADPH and thus may be linked to sugar metabolism in the dark. Previous studies suggested therefore that the two different systems may have different functions in plants. We now report that there is a previously unrecognized functional redundancy of thioredoxin-*f*1 and NTRC in regulating photosynthetic metabolism and growth. In Arabidopsis mutants, combined - but not single - deficiencies of thioredoxin-*f*1 and NTRC led to severe growth inhibition and perturbed light acclimation, accompanied by strong impairments of Calvin-Benson-cycle activity and starch accumulation. Light-activation of key-enzymes of these pathways, fructose-1,6-bisphosphatase and ADP-glucose pyrophosphorylase, was almost completely abolished. The subsequent increase in NADPH/$NADP^+$ and ATP/ADP ratios led to increased nitrogen assimilation, NADP-malate dehydrogenase activation and light-vulnerability of photosystem I core-proteins. In an additional approach, reporter studies show that Trx *f*1 and NTRC proteins are both co-localized in the same chloroplast substructure. Results provide genetic evidence that light and NADPH dependent thiol-redox systems interact at the level of thioredoxin-*f*1 and NTRC to coordinately participate in the regulation of Calvin-Benson-cycle, starch metabolism and growth in response to varying light conditions.

INTRODUCTION

Reversible disulfide-bond formation between two cysteine residues regulates structure and function of many proteins in diverse organisms (Cook and Hogg, 2013). Thiol-disulfide exchange is controlled by thioredoxins (Trx), which are small proteins containing a redox-active disulfide group in their active site (Holmgren, 1985; Baumann and Juttner, 2002). The latter can be reduced to a dithiol by Trx reductases using NADPH or ferredoxin (Fdx) as electron donors. Due to their low redox midpoint potential, reduced Trxs are able to reductively cleave disulfide-bonds in many target proteins and, thus, modulate their functions.

Plants contain the most versatile Trx system found in all organisms with respect to the multiplicity of different isoforms and reduction systems (Buchanan and Balmer, 2005; Nikkanen and Rintamäki, 2014; Geigenberger and Fernie, 2014). The Arabidopsis genome contains a complex family of Trxs, including up to 20 different isoforms grouped into seven subfamilies (Schuermann and Buchanan, 2008; Dietz and Pfannschmidt, 2011). Trxs *f*1-2, *m*1-4, *x*, *y*1-2 and *z* are located exclusively in the chloroplast, Trx *o* exclusively in the mitochondria, while the eight Trx *h* representatives are distributed between the cytosol, nucleus, endoplasmic reticulum (ER), and mitochondria (Meyer et al., 2012). The different Trxs can be reduced by two different redox systems, dependent on Fdx and Fdx-Trx reductase (FTR) in the chloroplast or NADPH and NADPH-Trx reductase (NTRA and NTRB) in other cell compartments (Buchanan and Balmer, 2005). More recently, a third type of NADPH-Trx reductase (NTRC) has been identified which forms a separate Trx system in the chloroplast (Serrato et al., 2004; Perez-Ruiz et al., 2006). NTRC is a bimodular enzyme containing both an NTR and Trx domain on a single polypeptide (Serrato et al., 2004). Its catalytic unit is a homodimer, transferring electrons from NTR to Trx domains via inter-subunit pathways (Pérez-Ruiz and Cejudo, 2009). In vitro studies suggest that NTRC is a Trx with its own Trx reductase, since it has not been shown to interact with other free Trxs (Perez-Ruiz et al., 2006; Bohrer et al., 2012).

In chloroplasts, Trxs are reduced via FTR in a light-dependent manner, using photosynthetic electrons provided by Fdx. The Fdx-Trx system with Trxs *f* and *m* was originally discovered as a mechanism for the regulation of the Calvin-Benson cycle,

ATP synthesis and NADPH export in response to light-dark changes (Buchanan et al., 1979; Buchanan, 1980). In numerous biochemical studies performed in vitro, the roles of Trxs *f* and *m* were extended to the regulation of many other chloroplast enzymes involved in various pathways of primary metabolism (Buchanan and Balmer, 2005; Meyer et al., 2012). In-vitro experiments with purified proteins revealed differences in biochemical specificities to different types of Trxs. Enzymes of the Calvin-Benson cycle were found to be exclusively regulated by *f*-type Trxs (Collin et al., 2003; Michelet et al., 2013; Yoshida et al. 2015), while key-enzymes involved in related pathways such as starch synthesis (Fu et al., 1998; Ballicora et al., 2000; Geigenberger et al., 2005; Thormählen et al., 2013), starch degradation (Mikkelsen et al., 2005; Valerio et al., 2011; Seung et al., 2013; Silver et al., 2013), fatty acid synthesis (Sasaki et al., 1997), amino acid synthesis (Lichter and Häberlein, 1998; Choi et al., 1999; Balmer et al., 2003), chlorophyll synthesis (Ikegamie et al. 2007; Luo et al. 2012), NADPH export (Collin et al., 2003; Yoshida et al. 2015) and oxidative pentose-phosphate pathway (Nee et al. 2009) were found to be regulated by both Trxs *f* and *m*, with *f*- being in most cases more effective than *m*-type. Other plastidial isoforms belonging to the *x*- and *y*-types were found to be essentially involved in antioxidant functions, being efficient electron donors to 2-Cys peroxiredoxins (Prxs) and Prx Q, respectively, but unabel to activate carbon metabolism enzymes (Collin et al., 2003; Collin et al., 2004). The biochemical properties of Trx *z* are not fully resolved yet. While this new type of Trx has been identified to be part of the plastid-encoded RNA polymerase, implicating a role in the transcription of the plastome (Arsova et al., 2010), it has also been found to act as an electron donor for several antioxidant enzymes, indicating a role in plastid stress responses (Chibani et al., 2011).

While most of the results mentioned above are based on biochemical studies, little is known about the in-vivo relevance and specificity of the different chloroplast Trxs isoforms in planta. Recent progress in this area was made by using reverse genetic studies, including Arabidopsis mutants and transgenic plants. Intriguingly, these genetic studies revealed specific roles of *m*-type Trxs in regulating photosynthetic electron transport and developmental processes, rather than its expected roles in primary metabolism. Arabidopsis lines with combined under-expression of Trxs *m*1, *m*2 and *m*4 were defective in the biogenesis of photosystem II (Wang et al., 2013),

single mutants with deletions in Trx *m*4 were affected in alternative photosynthetic electron transport pathways (Courteille et al., 2013), while deletions in Trx *m*3 affected meristem development (Benitez-Alfonso et al., 2009). In addition to this, Arabidopsis mutants with deletions in Trx *f*1 leading to a more than 97% decrease in Trx *f* protein level showed alterations in diurnal starch accumulation, rather than any changes in photosynthetic parameters and growth (Thormählen et al., 2013). This is surprising, given the exclusive regulation of individual steps of the carbon fixation cycle by Trx *f*1 in vitro (Collin et al., 2003; Michelet et al., 2013).

Compared to the Fdx-Trx system, relatively little is known on the more recently identified chloroplast NADPH dependent NTRC system, which uses NADPH as a source of electrons. So far only a few targets have been identified to be regulated by NTRC, with 2-Cys Prxs involved in H_2O_2-detoxification (Perez-Ruiz et al., 2006), ADPGlc pyrophosphorylase (AGPase) the key enzyme of starch biosynthesis (Michalska et al., 2009; Lepisto et al., 2013) and enzymes of chlorophyll biosynthesis (Richter et al., 2013; Perez-Ruiz et al., 2014) being the most elaborated ones. Regulation of these processes by NTRC was confirmed in planta by analyzing an insertional knockout mutant of NTRC, revealing (i) a decreased 2-Cys-Prx redox-status and impaired H_2O_2-detoxification (Perez-Ruiz et al., 2006), (ii) an attenuation of redox-activation of AGPase and starch accumulation (Michalska et al., 2009; Lepisto et al., 2013), and (iii) impaired GluTR1, CHLM and Mg-chelatase activities together with decreased chlorophyll levels (Richter et al., 2013; Perez-Ruiz et al., 2014). Since most of these effects were operational in the dark, this suggests a role of NTRC to regulate these pathways independently of light. In addition to the NADPH-dependent NTRC system, 2-Cys Prx and AGPase have also been found to be regulated by the light-dependent Fdx-Trx system with Trx *x* (Collin et al. 2003; Bohrer et al. 2012) and Trx *f*1 (Thormählen et al., 2013), respectively. However, little is known on the interrelation of light and NADPH dependent chloroplast redox systems in regulating these targets.

In this report, the interrelation between Trx *f*1 and NTRC in regulating plant metabolism and growth was investigated by using a genetic approach. Analysis of an Arabidopsis *trxf*1 *ntrc* double mutant shows that combined inactivation of Trx *f*1 and NTRC leads to a strong inhibition in light-activation of the Calvin-Benson cycle and

related metabolic activities resulting in a severe limitation of growth, while these responses were not or only weakly expressed in the single mutants. Reporter studies show that both Trx *f*1 and NTRC are expressed in the same tissues during development and are co-localized in the same chloroplast substructure. This provides evidence for a previously unknown redundant function of Trx *f*1 and NTRC in regulating photosynthetic metabolism and growth in response to varying light conditions.

RESULTS

Combined inactivation of Trx *f*1 and NTRC leads to a severe growth phenotype

To analyze the interrelation between Trx *f*1 and NTRC in regulating growth and metabolism of Arabidopsis plants, the well-characterized *trxf1* (SALK_128365; Thormählen et al., 2013) and *ntrc* (SALK_012208; Serrato et al., 2004; Pérez-Ruiz et al., 2006) T-DNA insertion lines were crossed to generate a *trxf1 ntrc* double mutant. A homozygous *trxf1 ntrc* line was identified, where T-DNA insertions were present in both genomic alleles (Fig. 1A), while protein content of both Trx *f*1 and NTRC were strongly decreased to detection limit (Fig. 1B). In comparison to this, expression of NTRC and Trx *f*1 was still detectable in the *trx f1* and *ntrc* single mutants, respectively, although Trx *f*1 protein levels were found to be slightly lower in the *ntrc* background than in the wild-type (Fig. 1B). In the Western blots of Fig. 1B, a Trx *f* antibody was used that gives similar signals with Trx *f*1 and Trx *f*2 (Thormählen et al., 2013), indicating that Trx *f*1 is the predominant Trx *f* isoform in Arabidopsis.

As previously reported, *trxf1* (Thormählen et al., 2013) and *ntrc* single mutants (Perez-Ruiz et al., 2006; Lepisto et al., 2013) showed no or moderate growth phenotypes, respectively, when grown in a 8 h photoperiod at 160 µmol photons m^{-2} s^{-1} light intensity (Fig. 2B). In contrast to this, growth of the *trxf1 ntrc* double mutant was very severely perturbed, when compared to the wild-type or the single mutants (Fig. 2B). The rosette fresh-weights of the *trxf1 ntrc* double mutant decreased to below 2% of wild-type level, while those of the *ntrc* mutant decreased to 25% and those of the *trxf1* mutant remained unaltered (Fig. 2H). Despite this very strong growth defect, *trxf1 ntrc* mutant plants were viable and produced seeds under these conditions (Fig. 2G). Interestingly, the extent of the growth phenotypes differed depending on the length of the photoperiod and the light intensity (Figs. 2 A-F). When the length of the photoperiod was decreased from 8 to 4 h light, rosette fresh-weights decreased significantly to 80% and 15% of wild-type level in the *trxf* and *ntrc* single mutants, respectively, and to levels below the detection limit in the *trxf1 ntrc* double mutant (Fig. 2H). Conversely, an increase in the length of the photoperiod from 8 to 24 h led to a partial relieve in the growth retardation of both the *ntrc* and the *trxf1 ntrc* mutant. In the *ntrc* mutant, rosette fresh-weights increased from 25 to 50% of wild-

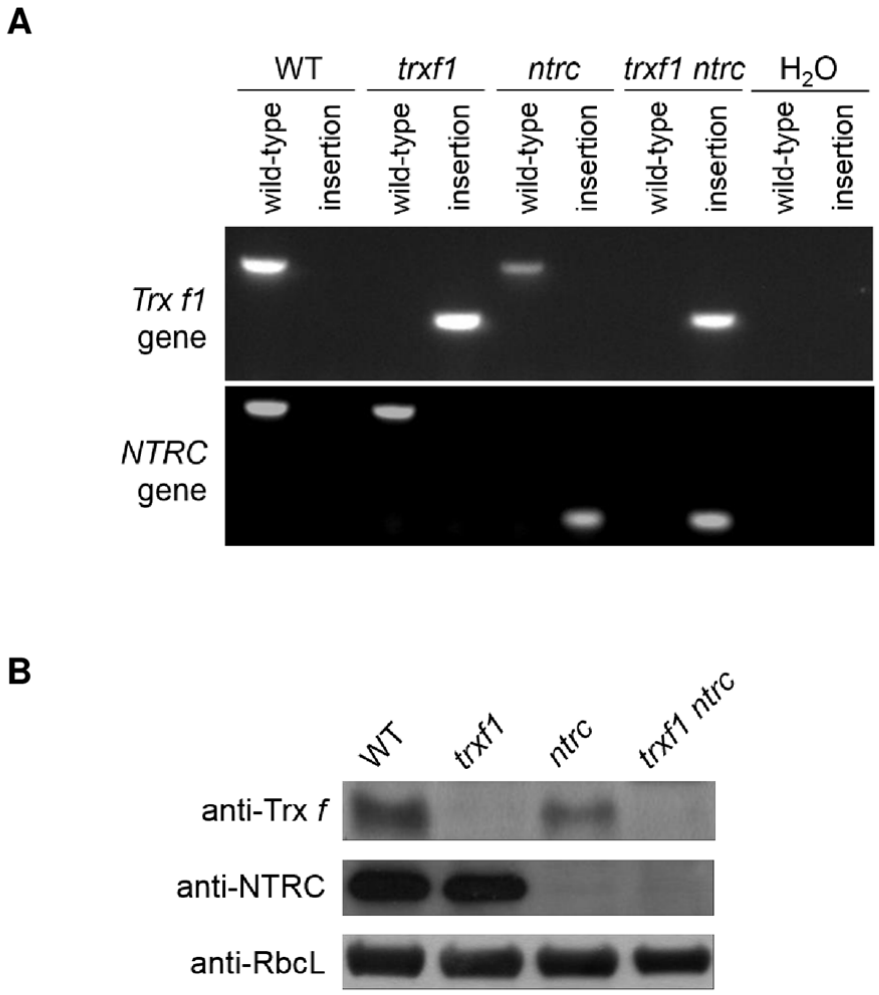

Figure 1: Molecular characterization of *trxf1*, *ntrc* and *trxf1 ntrc* Arabidopsis mutants compared to wild-type. **(A)** Genotyping by PCR analysis with different primer combinations (wild-type or insertion) for the identification of T-DNA insertions in *Trx f1* and *NTRC* genes. **(B)** Detection of Trx *f* and NTRC proteins using Western blot analysis. Representative Western blots are shown of measurements, which were performed in leaves of 5-week old plants grown in an 8h-day with 160 µmol photons m^{-2} s^{-1} light regime harvested 4 h into the light period. Rubisco protein level is shown as control.

type level in 16 h and 24 h, compared to 8 h photoperiods (Fig. 2H), in agreement with previous studies (Lepisto et al., 2009). The *trxf1 ntrc* double mutant showed no significant change in fresh-weight when the photoperiod was increased from 8 h to 16 h light, but there was an increase from 1 to 3% of wild-type level when the photoperiod was increased from 16 h to 24 h light (Fig. 2H). Also a change in the light

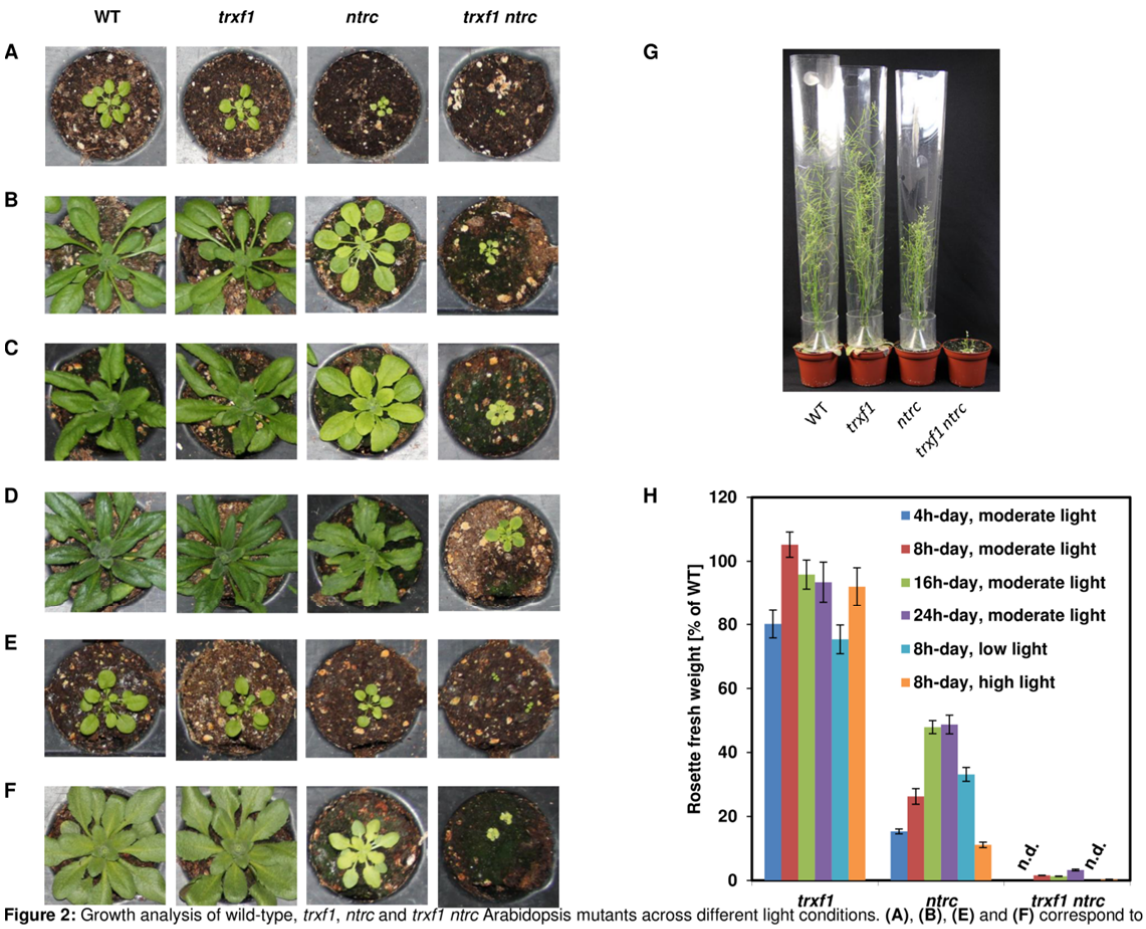

Figure 2: Growth analysis of wild-type, *trxf1*, *ntrc* and *trxf1 ntrc* Arabidopsis mutants across different light conditions. **(A)**, **(B)**, **(E)** and **(F)** correspond to 5 week-old plants, while **(C)** and **(D)** correspond to 4 week-old plants, and **(G)** to 7 week-old plants. In the first week, plants - except (**G**) - were grown in an 8 h-day and moderate light intensity regime before they were transferred for additional 3-4 weeks to the conditions indicated below: **(A)** 4 h-day and moderate light intensity , **(B)** 8 h-day and moderate light intensity, **(C)** 16 h-day and moderate light intensity, **(D)** 24 h-day and moderate light intensity, **(E)** 8 h-day and low light intensity, **(F)** 8 h-day and high light intensity, and **(G)** 16 h-day in greenhouse. In **(H)**, rosette fresh-weights of plants corresponding to the conditions shown in **(A)** to **(F)** are given as percent of wild-type levels in the respective conditions. Results are the mean ± SE, *n* = 30-86 (wild-type), 15-44 (*trxf1*), 5-44 (*ntrc*) or 9-111 (*trxf1 ntrc*) different plants. All values are significantly different from wild-type according to the Student's *t*-test ($P<0.05$), except the *trxf1* mutant in 8 h-, 16 h- and 24 h-day regimes at moderate and high light intensities (see Suppl. Table S1). Low light intensity = 30 µmol photons m^{-2} s^{-1}; moderate light intensity = 160 µmol photons m^{-2} s^{-1}; high light intensity = 950 µmol photons m^{-2} s^{-1}; n.d. = not detectable (fresh-weight values were below the detection limit)

intensity at 8 h-photoperiod affected the growth phenotype of the mutants. When the light intensity was decreased from 160 µmol photons m^{-2} s^{-1} to 30 µmol photons m^{-2} s^{-1}, the rosette fresh weights dropped significantly to 75 and 35% of wild-type level in the *trxf1* and *ntrc* mutants, respectively, and to levels below the detection limit in the *trxf1 ntrc* double mutant (Fig. 2H). When the light intensity was increased from 160 to 950 µmol photons m^{-2} s^{-1}, rosette fresh-weights dropped severely in the *trxf1 ntrc* mutant, moderately in the *ntrc* mutant, while no effect was observed in the *trxf1* mutant, compared to wild-type (Fig. 2H). Overall, the results show that knockout of Trx *f*1 leads to a severe growth inhibition in the *ntrc*, but not in the wild-type background, suggesting a functional redundancy of both redox systems.

Combined deficiency of Trx *f*1 and NTRC leads to a strong impairment of photosynthesis

To investigate whether the severe growth phenotype of the *trxf1 ntrc* mutant is due to an effect on photosynthesis, CO_2 assimilation rates were measured in leaves of the different genotypes grown in an 8 h photoperiod at 160 µmol photons m^{-2} s^{-1} light intensity using an open gas-exchange system. The light response-curves at ambient CO_2 are shown in Fig. 3A. At light intensities between 150 and 1000 µmol photons m^{-2} s^{-1}, CO_2 fixation rates were strongly decreased in the *trxf1 ntrc* mutant relative to the wild-type, the decrease being light intensity-dependent: 80% at 150, 60% at 200-300, 50% at 400-600, and 33% at 800-1000 µmol photons m^{-2} s^{-1}. At light intensities between 50-100 µmol photons m^{-2} s^{-1}, CO_2 assimilation rates were below the respiration rate in the double mutant, but not in the wild-type, the light compensation point switching from 20 µmol photons m^{-2} s^{-1} in the wild-type to 120 µmol photons m^{-2} s^{-1} in the double mutant. In the dark, CO_2 release rates were 4-fold higher in the double mutant compared to wild-type. In contrast to the double mutant, the single mutants showed no (*trxf1*) or only slight changes (*ntrc*) in CO_2 assimilation rates, compared to wild-type. Deletion of NTRC led to a slight decrease in CO_2-assimilation rates at all light intensities, which was statistically significant at 50 and 200 µmol photons m^{-2} s^{-1} using the Student´s *t*-test (Suppl. Table S2) and for all light intensities using the two-way Anova test (Fig. 3A), confirming previous studies (Lepisto et al., 2009). Overall, the results show that inactivation of Trx *f*1 led to a strong decrease in CO_2 fixation rates in the *ntrc*, but not in the wild-type background, lending further support to the proposal of a functional redundancy of both systems to regulate the CO_2 fixation rate.

In Fig. 3B, leaf transpiration rates are shown across different light intensities and genotypes. Compared to wild-type, there was a strong (up to 8-fold) increase in transpiration rates in the *trxf1 ntrc* mutant, while the single mutants behaved like the wild-type at all light conditions tested. Similar results were observed for stomal conductance (data not shown) and intercellular CO_2 concentration (Fig. 3C), both parameters being strongly increased in the double mutant relative to the wild-type. These results show that the lower rate of CO_2 fixation caused by the combined deficiency of Trx *f*1 and NTRC is not due to a restriction in CO_2 uptake rates or a

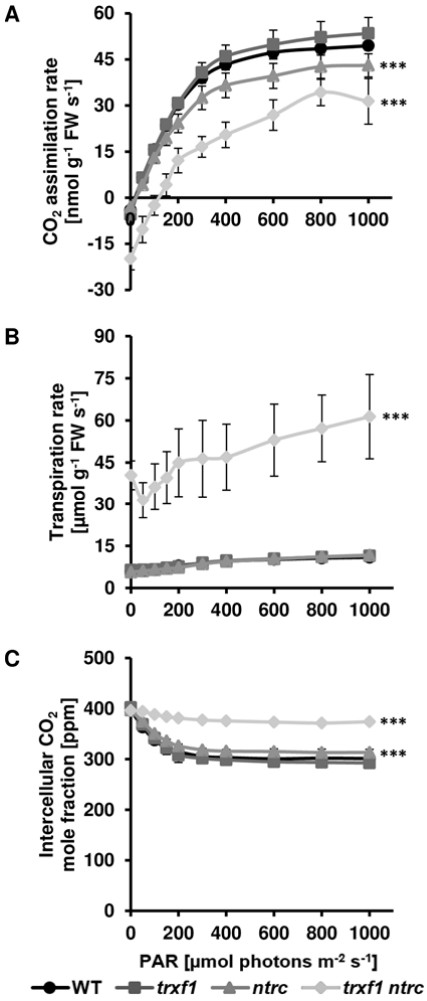

Figure 3: Changes in gas-exchange parameters in leaves of *trxf1*, *ntrc* and *trxf1 ntrc* Arabidopsis mutants compared to wild-type. **(A)** CO_2 assimilation rate, **(B)** transpiration rate, and **(C)** intercellular CO_2 concentration were measured at different light intensities in leaves from plants growing in an 8 h photoperiod with 160 µmol photons m^{-2} s^{-1}. Results are the mean ± SE, *n* = 10 (wild-type) or 5 (mutants) different plant replicates. *: P<0.05, **: P<0.01, ***: P<0.001 (according to two-way analysis of variance [Anova)], Tukey test); for further statistical analysis see Suppl. Table S2;
PAR = photosynthetic active radiation

decrease in internal CO_2 concentrations, but most likely to a direct inhibition of the CO_2-fixation cycle.

To investigate whether the inhibition of CO_2-assimilation is accompanied by changes in photosynthetic light reactions, chlorophyll fluorescence parameters were measured by pulse-amplitude modulation (PAM) fluorimetry. A significant decrease of maximal (F_v/F_m) and effective quantum yield of PS II (Φ_{PSII}) was observed in the double mutant relative to the single mutants or the wild-type (Figs. 4A and 4B), indicating that the combined deficiency of Trx *f*1 and NTRC led to a strong impairment of PSII functionality and photosynthetic electron transport rates. Correspondingly, quantum yields of regulated (ΦNPQ) and non-regulated (ΦNO) energy dissipation (Fig. 4B) were strongly increased in the double mutant. Similar to previous studies (Lepisto et al., 2009; Thormählen et al., 2013), no changes in chlorophyll fluorescence parameters were found in the *trxf1* mutant, while the *ntrc* mutant revealed moderate but significant changes in Φ_{PSII} and ΦNPQ, relative to the wild-type (Fig. 4B).

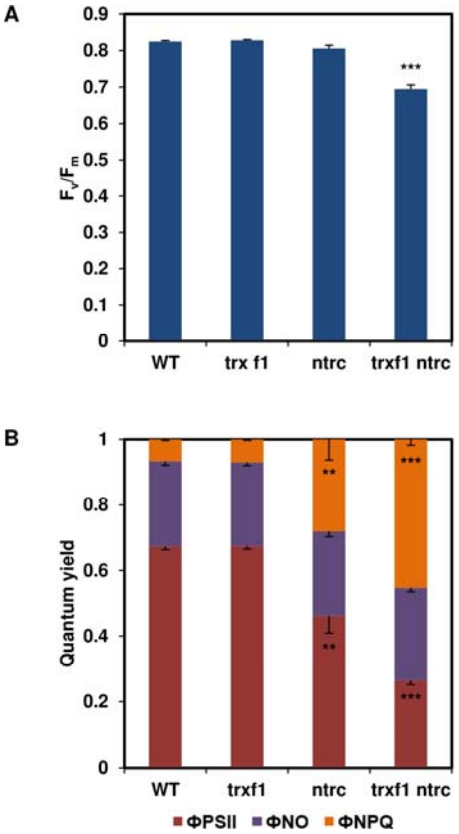

Figure 4: Changes in chlorophyll fluorescence parameters in leaves of *trxf1*, *ntrc* and *trxf1 ntrc* Arabidopsis mutants compared to wild-type. Plants growing in an 8 h photoperiod with 160 µmol photons m^{-2} s^{-1} were dark adapted for 10 min, before exposure of a far red light saturation pulse (5,000 µmol m^{-2} s^{-1} for 0.8 s) to single leaves. Afterwards the maximal chlorophyll a fluorescence was quenched by electron transport with an actinic red light of 166 µmol photons m^{-2} s^{-1}. Within 10 min the steady state was reached and another saturation pulse was given. In the end, **(A)** the maximal PSII (F_v/F_m), and **(B)** the effective PSII (Φ_{PSII}), the non-regulated energy dissipation (Φ_{NO}) and the regulated energy dissipation (Φ_{NPQ}) quantum yields were calculated. Results are means ± SE, *n* = 11 different plants.

*: P<0.05, **: P<0.01, ***: P<0.001 (according to Student's *t*-test)

We further investigated whether impaired photosynthetic light reactions were accompanied by decreased abundance of proteins involved in photosynthetic electron transport (Fig. 5). Western blot analyses showed that combined deficiency of Trx *f*1 and NTRC led to a strong decrease in proteins of the PSI complex (PsaA and PsaB) down to approx. 25% of wild-type level and to more moderate decreases in proteins of PSII (PsbD), cytochrome b6-f (PetC), light-harvesting (Lhca1 and Lhcb1) and ATPase complexes (Atpß). In comparison to this, the *trxf1* and *ntrc* single mutants were only weakly affected. Chlorophyll content was slightly decreased in the *trxf1* mutant, and down to 55 and 45% of wild-type level in the *ntrc* single and *trxf1 ntrc* double mutant, respectively (Suppl. Fig. S1). This confirms previous studies showing chlorophyll levels to be decreased by 50% in the *ntrc* mutant relative to the wild-type (Perez-Ruiz et al., 2006; Lepisto et al., 2009), while a combined deficiency of Trx *f*1 and NTRC only led to minor additional effects (Suppl. Fig. S1).

Combined deficiency of Trx *f*1 and NTRC affects NADP reduction and adenylate energy states

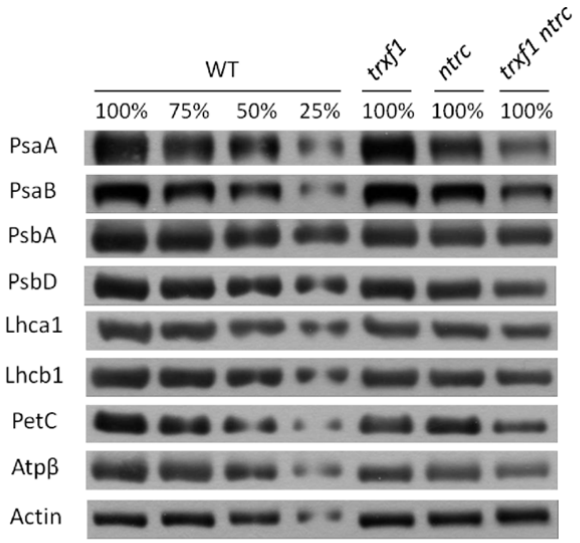

Figure 5: Changes in the levels of proteins involved in photosynthetic electron transport and ATP synthesis in leaves of *trxf1*, *ntrc* and *trxf1 ntrc* Arabidopsis mutants compared to wild-type. PsaA, PsaB, PsbA, PsbD, PetC, Lhca1, Lhcb1 and Atpß proteins were detected using specific antibodies. Representative Western blots are shown from 5-week old plants growing in an 8h-day with 160 µmol photons m^{-2} s^{-1} light regime harvested 4 h into the light period. In the wild-type, different amounts of samples were loaded (25-100%) for comparison. Actin protein level is shown as control.

The Calvin–Benson cycle uses most of the ATP and NADPH delivered by the photosynthetic light reactions (Michelet et al., 2013). To investigate the relationship between photosynthetic activity and the function of the Calvin-Benson cycle, the levels of NAD(P)H, $NAD(P)^+$, ATP and ADP were analyzed in leaves of wild-type and the different redox mutants (Fig. 6). In wild-type plants, the sum of NADPH and $NADP^+$ increased at the end of the day relative to the end of the night (Fig. 6A), while the NADPH/$NADP^+$ ratio decreased (Fig 6B), confirming previous studies (Liu et al., 2008; Beeler et al., 2014; Lintala et al., 2014). The light-induced decrease in the NADPH/$NADP^+$ ratio is probably attributable to the Calvin-Benson cycle being activated under these conditions. In the *trxf1 ntrc* mutant, the diurnal changes in the sum of NADPH and $NADP^+$ levels were strongly attenuated (Fig. 6A), while there was a clear increase in the NADPH/$NADP^+$ ratio at the end of the day (3-fold) and at the end of the night (2-fold), compared to wild-type (Fig. 6B). No changes were observed in the *trxf1* mutant while in the *ntrc* mutant the NADPH/$NADP^+$ ratio was slightly but significantly increased (Figs. 6A and 6B). The wild-type also showed diurnal changes in the sum of NADH and NAD^+ (Fig. 6C) and in the NADH/NAD^+ ratio (Fig. 6D), with the former decreasing and the latter increasing towards the end of the day. In the *trxf1 ntrc* mutant, the sum of NADH and NAD^+ was further decreased, while the NADH/NAD^+ ratio further increased, compared to wild-type.

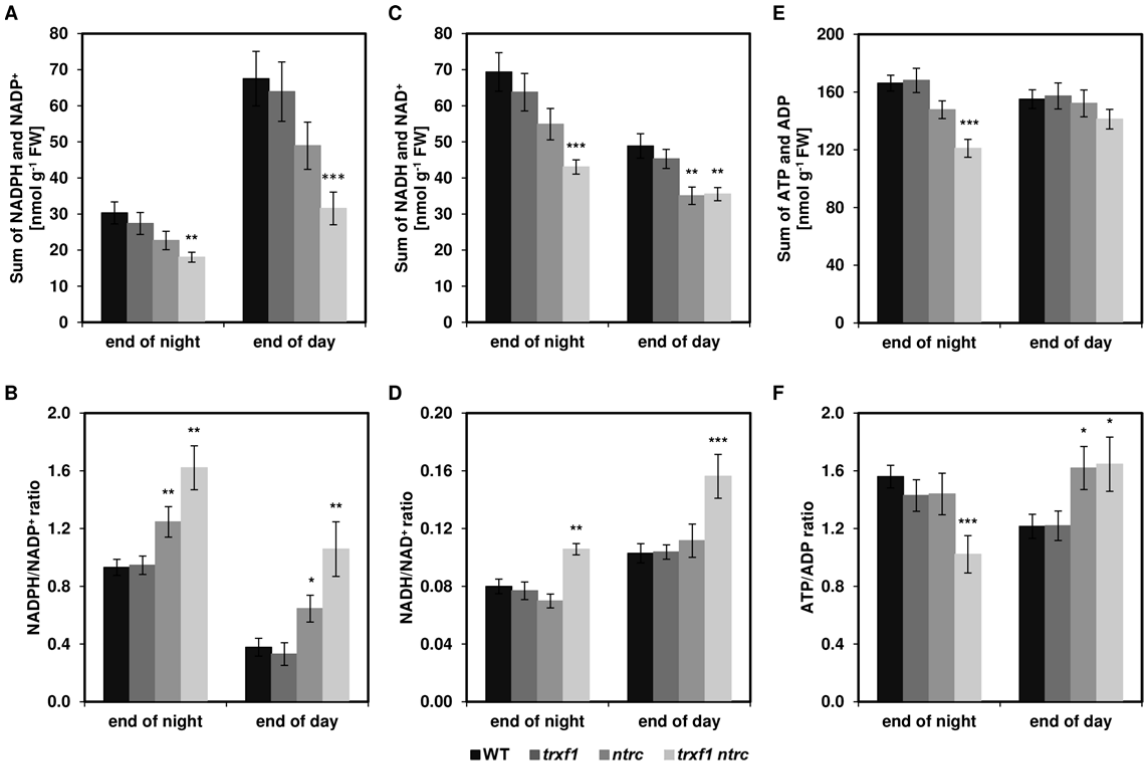

Figure 6: Changes in nucleotide levels in leaves of *trxf1*, *ntrc* and *trxf1 ntrc* Arabidopsis mutants compared to wild-type. **(A)** Sum of NADPH and NADP, **(B)** NADPH/NADP ratio, **(C)** sum of NADH and NAD, **(D)** NADH/NAD ratio, **(E)** sum of ATP and ADP, and **(F)** ATP/ADP ratio were measured in leaves harvested at the end of day and end of night. Results are means ± SE, n = 20-30 (wild-type) or 10-15 (mutants) independent plant replicates. Plants were grown in an 8 h photoperiod with 160 µmol photons m^{-2} s^{-1}. *: P<0.05, **: P<0.01, ***: P<0.001 (according to Student's *t*-test).

In the wild-type, the diurnal changes in NADP redox state were accompanied by corresponding changes in adenylate energy state, with ATP/ADP ratios being decreased at the end of the day as compared to the end of the night (Fig. 6F). A similar decrease in the ATP/ADP ratio from 1.5 to 1.2 in response to light was found in previous studies with leaves of wild-type Arabidopsis plants (Carrari et al. 2005). This is most probably attributable to light-activation of the Calvin-Benson cycle and other ATP-consuming biosynthetic processes. In the *trxf1 ntrc* mutant, diurnal changes in both adenylate levels (Fig. 6E) and ATP/ADP ratios (Fig. 6F) were opposite to the wild-type, being increased during the day relative to the night, while the *trxf1* and *ntrc* single mutants were largely similar to wild-type (Figs. 6E and 6F).

Overall these results show that a combined deficiency of Trx *f*1 and NTRC causes major alterations in both NADPH/$NADP^+$ and ATP/ADP ratios during the day, indicating that the primary cause for the strong impairment of photosynthesis is an inhibition of the Calvin-Benson cycle rather than the light reactions.

Combined deficiency of Trx *f*1 and NTRC strongly impairs redox-activation of

fructose-1,6-bisphosphatase while having no inhibitory effect on redox-activation of NADP-malate dehydrogenase

The above described results show that the combined deficiency of Trx *f*1 and NTRC causes impairment of photosynthetic parameters, the diurnal oscillation of energy availability and carbon fixation rate. We then analyzed whether this could be due to direct effects on enzymes of the Calvin-Benson cycle or NADPH export from the chloroplast. To this end we focused on FBPase and NADP-MDH, representing key-regulatory steps of these processes and classical targets of Trx *f* and Trx *m*, respectively (Buchanan et al. 1979). Chloroplast FBPase (cpFBPase) is known to be subject to exquisite light-activation via the Fdx-Trx *f* system, leading to reduction of an intra-molecular disulfide that promotes activation of the enzyme (Zimmermann et al., 1976; Buchanan et al. 1979). To analyze the effect of a combined deletion of NTRC and Trx *f*1 on redox regulation of FBPase, the redox status of the chloroplast enzyme was analyzed in vivo by labeling of thiol groups with the alkylating agent MM-PEG_{24}, which adds 1.5 kDa per thiol, thus causing a switch of the electrophoretic mobility of the reduced form of the enzyme as compared to the oxidized form. In the wild-type, cpFBPase protein was completely oxidized at the end of the night, while more than 50% of the protein was in the reduced state at the end of the day (Fig. 7A), confirming light-induced reduction of its intra-molecular disulfide in vivo. This response was strongly modified in the redox mutants. At the end of the day, the ratio of reduced to oxidized cpFBPase protein was substantially decreased in *trxf1* and *ntrc* single mutants relative to the wild-type, while there was an even stronger decrease in the double mutant (Fig. 7A). No changes were observed between the genotypes at the end of the night. Results from four independent experiments were quantified and are summarized in Fig. 7B, showing that the ratio of reduced to oxidized cpFBPase protein decreased significantly by 40% in *trxf1*, 20% in *ntrc* and 70% in *trxf1 ntrc* mutants relative to the wild-type, indicating an additive effect in the double mutant. Finally, it was noticed that the content of cpFBPase protein in the double mutant was slightly decreased as compared with the wild-type or single mutants (Fig. 7A) suggesting minor effects on cpFBPase protein turnover in addition to post-translational thiol-disulfide modulation.

We then investigated whether a deficiency in Trx *f*1 and NTRC also affects FBPase

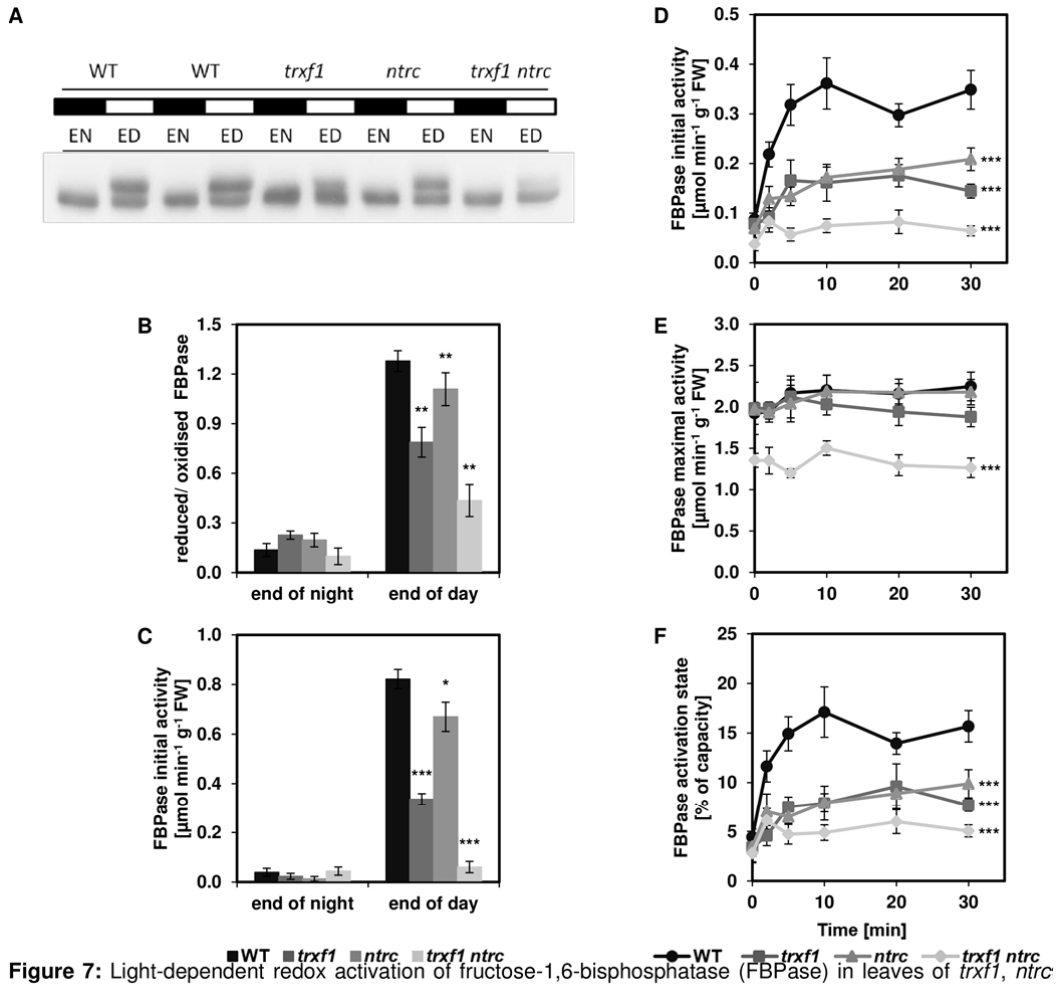

Figure 7: Light-dependent redox activation of fructose-1,6-bisphosphatase (FBPase) in leaves of *trxf1*, *ntrc* and *trxf1 ntrc* Arabidopsis mutants compared to wild-type. **(A)** and **(B)** show the thiol-disulfide reduction state of chloroplast FBPase in leaves harvested at the end of night (EN) and end of day (ED) analyzed by using gel-shift assays: **(A)** Representative gel-shift blot using an antibody specific for chloroplast FBPase, and **(B)** calculated ratio of reduced to oxidized FBPase. **(C)** Corresponding initial enzyme activity of FBPase (assay without DTT) in leaves harvested at the end of night (EN) and end of day (ED). **(D)** to **(F)** Transient light activation of FBPase during a detailed time course. At the end of the night (0 min), plants were illuminated for different time-periods (2, 5, 10, 20 and 30 min) to measure FBPase activity using different assay conditions: **(D)** Initial activity without DTT additions in the assay, **(E)** maximal activity with 10 mM DTT included in the assay, and **(F)** estimated redox-activation state (initial/maximal activity*100). Results are means ± SE, *n* = 8 (wild-type) or 4 (mutants) independent plant replicates **(B)**, *n* = 20 (wild-type) or 10 (mutants) independent plant replicates **(C)**, and *n* = 10 (wild-type) or 4-6 (mutants) independent plant replicates **(D)** to **(F)**. All plants were grown in an 8 h photoperiod with 160 µmol photons m^{-2} s^{-1}. *: P<0.05, **: P<0.01, ***: P<0.001, according to Student's *t*-test **(B)** and **(C)** or two-way analysis of variance [Anova] Tukey test **(D)** to **(F)**, see Suppl Table S3**.** Estimation of the redox-activation state from enzyme assays **(F)** and the directly measured thiol-disulfide state of the protein **(B)** yielded different absolute values, which is most likely due to additional factors affecting FBPase activity during the enzyme assays.

enzyme activity. In leaves of the wild-type, FBPase activity was very low at the end of the night and increased 20-fold towards the end of the day (Fig. 7C), confirming previous studies on the light activation of cpFBPase (Zimmermann et al., 1976; Chiadmi et al., 1999). This response was strongly attenuated in the redox mutants. At

the end of the day, FBPase activity was progressively decreased down to 40, 80 and 7% of wild-type level in *trxf1*, *ntrc* and *trxf1 ntrc* mutants, respectively, while there were no significant changes between these genotypes at the end of the night. In the double mutant, no significant changes between nocturnal and day-time FBPase activity were observed, indicating that light activation of FBPase has been abolished. The data also show a correlation between FBPase activity and FBPase redox-state across different genotypes and day-night conditions (compare Figs. 7B and 7C), confirming the major role of thiol-disulfide modulation in regulating FBPase enzyme activity in-vivo. It should be noted that the FBPase activity was measured in crude extracts which will likely overestimate the residual chloroplastic activity in the dark, as the redox-insensitive cytosolic FBPase will contribute to the measured activity. However, analysis of Arabidopsis mutants lacking cytosolic FBPase show that under these conditions 80% of the FBPase activity in crude leaf extracts is due to chloroplastic cpFBPase (Rojas-Gonzalez et al. 2015).

To investigate transient light-activation of FBPase in a detailed time course, FBPase activity was analyzed in leaves 0, 2, 5, 10, 20 and 30 min after illumination. As shown in Fig. 7D, light led to a rapid increase in FBPase activity, reaching half-maximal activity within 1 min after the start of illumination in the wild-type. Compared to wild-type, the increase in FBPase activity was significantly delayed by approx. 50% in *trx f1* and *ntrc* single mutants, reaching half-maximal activities 5 and 10 min after the start of illumination, respectively. Between 10 and 30 min, FBPase activity showed no further increase or increased only slightly, with *trxf1* and *ntrc* mutants both saturating at approx. 50% of wild-type level. Intriguingly, combined deficiency of Trx *f*1 and NTRC led to a complete loss in light-activation of FBPase, with the double mutant showing no significant increase in FBPase activity upon illumination. When FBPase activity was measured in the presence of 10 mM DTT in the assay medium to fully reduce the regulatory disulfide of the enzyme, no significant changes were detected in the different genotypes and light conditions, except a slight decrease of the maximal FBPase activity in the *trxf1 ntrc* mutant compared to wild-type and single mutants (Fig. 7E). The ratio between the activities in the two assay conditions (minus DTT versus plus DTT) is shown as a calculated redox-activation state in Fig. 7F. The changes in the estimated redox-activation state followed similar curves as the initial activities measured without DTT (compare Figs. 7D and 7F). The results show that

knockout of Trx *f*1 led to a decreased efficiency in light activation of FBPase which is in-line with earlier studies showing that chloroplast FBPase is redox-activated by *f*-type Trx in vitro (Collin et al., 2003). However, deletion of Trx *f*1 only led to a 50% inhibition in FBPase activation, which is similar to the degree of inhibition in the *ntrc* mutant, indicating that neither of these redox systems has an exclusive role in the redox-regulation of FBPase in-vivo. Moreover, the almost complete loss of light-dependent activation of FBPase in the *trxf1 ntrc* mutant strongly suggests the cooperative effect of Trx *f* and NTRC in FBPase redox regulation. A comparison between Figs. 7D and 7E also documents that the redox-sensitivity of the extracted FBPase protein itself was not compromised in the mutants relative to the wild-type.

For comparative purposes, we also measured the activity of NADP-MDH, a chloroplast enzyme involved in the export of NADPH to the cytosol via the malate valve (Scheibe, 2004) and being subject to activation by Trxs *f* and *m* in-vitro (Collin et al. 2003; Yoshida et al. 2015). In the wild-type, NADP-MDH initial activity was higher at the end of the day compared to the end of the night (Fig. 8A), confirming previous studies on the light-activation of this enzyme in the chloroplast stroma (Scheibe, 2004). Interestingly, this response was promoted rather than inhibited in the redox mutants. Compared to wild-type, *trxf1*, *ntrc* and *trxf1 ntrc* mutants showed increased activation of NADP-MDH during the day, while there were no substantial changes observed in the night. When NADP-MDH activity was measured in the presence of 10 mM DTT in the assay medium to fully reduce the regulatory disulfides of the enzyme, no substantial changes were detected across the different genotypes and light conditions (Fig. 8B). The ratio between the activities in the two assay conditions (minus DTT versus plus DTT) is shown as a calculated redox-activation state (Fig. 8C). It followed a similar curve as the initial activities measured without DTT (compare Figs. 8A and 8C). In the mutants, increased activation of NADP-MDH is probably due to increased chloroplast NADPH/$NADP^+$ ratios (Fig. 6), which promote NADP-MDH redox-activation indirectly by acting on the redox-potential of its regulatory disulfides (Faske et al., 1995).

Combined deficiency of Trx *f*1 and NTRC leads to decreased starch accumulation and decreased redox-activation of ADPGlc pyrophosphorylase

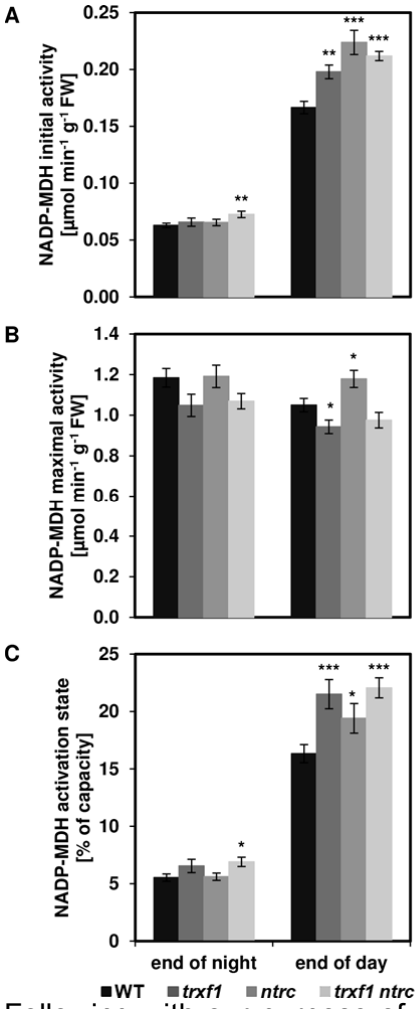

Figure 8: Light-dependent redox activation of NADP-dependent malate dehydrogenase (MDH) in leaves of *trxf1*, *ntrc* and *trxf1 ntrc* Arabidopsis mutants compared to wild-type. **(A)** Initial activity without DTT additions in the assay, **(B)** maximal activity with 10 mM DTT included in the assay, **(C)** redox-activation state (initial/maximal activity*100). Leaves were sampled at the end of night and end of day. Results are means ± SE, n = 24 (wild-type) or 12 (mutants) independent plant replicates. Plants were grown in an 8 h photoperiod with 160 µmol photons m^{-2} s^{-1}.
*: P<0.05, **: P<0.01, ***: P<0.001 (according to Student's *t*-test)

Following with our purpose of determining the function of Trx *f*1 and NTRC in redox regulation of different carbon metabolic pathways, we investigated the effect of the combined deficiency of Trx *f*1 and NTRC on the synthesis of photosynthetic end products, starch and sucrose. Wild-type leaves showed characteristic diurnal changes of starch (Fig. 9A) and sucrose levels (Fig. 9B), which increased by 3- and 2-fold, respectively, towards the end of the day. These diurnal changes were attenuated in the redox-mutants. At the end of the day, *trxf1*, *ntrc* and *trxf1 ntrc* mutants showed a progressive decrease in starch accumulation down to 80, 65 and 25% of wild-type levels, respectively (Fig. 9A), confirming previous studies showing attenuation of starch accumulation in *trxf1* (Thormählen et al., 2013) and *ntrc* single mutants (Michalska et al., 2009; Lepisto et al., 2013). The decrease in day-time starch content was additive in the double mutant (Fig. 9A), dropping to levels below those of the wild-type at the end of the night. At any time, the starch content in the double mutant did not exceed nocturnal wild-type levels. At the end of the night, *trxf1*, *ntrc* and *trxf1 ntrc* mutants showed a further progressive decrease in the remaining

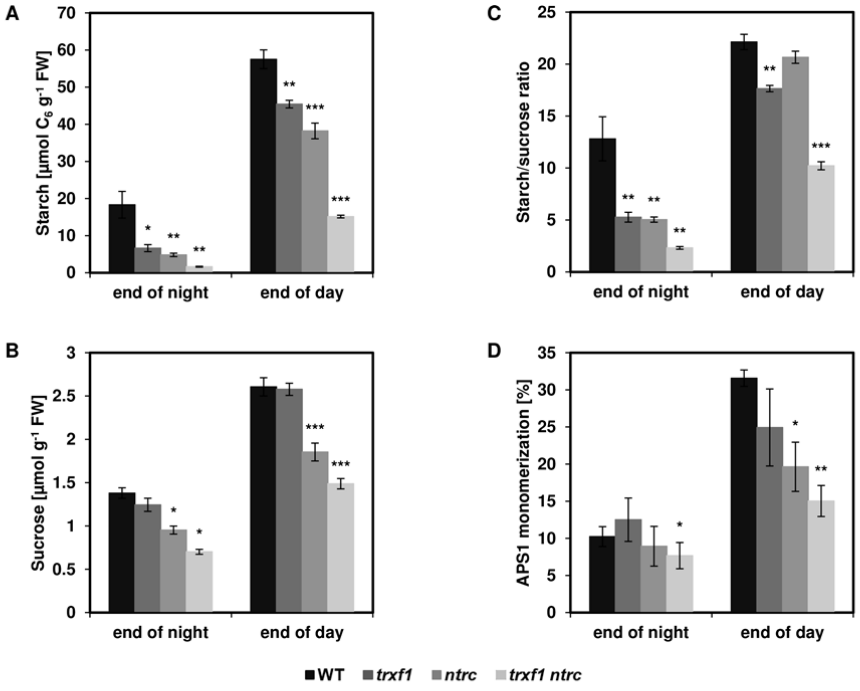

Figure 9: Changes in the accumulation of starch and sucrose and in the thiol-disulfide reduction state of the small subunits of ADP-glucose pyrophosphorylase (APS1) in leaves of *trxf1*, *ntrc* and *trxf1 ntrc* Arabidopsis mutants compared to wild-type. **(A)** Starch level, **(B)** sucrose level, **(C)** starch/sucrose ratio, and **(D)** APS1 monomerisation (APS1 monomer as percent of total APS1 [monomer + dimer]) were measured in leaves sampled at the end of night (EN) and end of day (ED). APS1 monomerisation was analyzed in non-reducing SDS gels, where reduced and oxidized APS1 can be separated as monomer and dimer, respectively. Results are means ± SE, $n = 8$ (wild-type) or 4 (mutants) independent plant replicates growing in an 8 h photoperiod with 160 µmol photons m^{-2} s^{-1}. *: P<0.05, **: P<0.01, ***: P<0.001 (according to Student's *t*-test)

starch content, reaching 35, 25 and less than 10% of the nocturnal wild-type level, respectively (Fig. 9A), showing that starch reserves were exhausted in the double mutant. The *trxf1 ntrc* mutant showed decreased accumulation of sucrose, which at a lower level was also affected in the *ntrc* mutant but not in the *trxf1* mutant (Fig. 9B). All mutants under analysis showed a decrease of the starch/sucrose ratio relative to the wild-type, the decrease being more pronounced in the *trxf1 ntrc* double mutant with 55% at the end of the day and 80% at the end of the night (Fig. 9C).

AGPase is a key-enzyme of starch synthesis, which is rapidly activated upon illumination by reduction of an intermolecular disulfide bond between the Cys-81 residues joining the two small subunits (APS1) of this heterotetrameric enzyme (Hendriks et al., 2003; Kolbe et al., 2005; Hädrich et al. 2012). To investigate whether the inhibition of starch synthesis in the different genotypes is due to decreased redox-activation of AGPase, monomerisation of APS1 was analyzed in leaves harvested at the end of the night and at the end of the day. As seen in previous studies (Hendriks et al., 2003), wild-type leaves revealed a strong increase in the monomerization of APS1 during the day, while APS1 was almost completely dimerized in the night (Fig. 9D). Compared to wild-type, light-dependent

monomerisation of APS1 was attenuated in the *trxf1* and *ntrc* single mutants (Fig. 9D), confirming results from earlier studies (Michalska et al., 2009; Thormählen et al., 2013). Compared to the single mutants, there was an additional attenuation of APS1 monomerisation in the *trxf1 ntrc* double mutant (Fig. 9D), indicating Trx *f*1 and NTRC to act additively on the reduction of APS1 in vivo.

Combined deficiency of Trx *f*1 and NTRC causes deep effects on metabolite levels including an increase in amino acids at the expense of organic acids

The above data clearly indicate the combined action of Trx *f* and NTRC on redox regulation of different aspects of carbon metabolism. The impairment of the regulation of the Calvin-Benson cycle and attendant starch synthesis in the mutants under investigation is expected to provoke changes of in-vivo metabolite levels indicative of regulatory steps in these pathways. In wild-type plants, the levels of 3-phosphoglycerate (3PGA) (Fig. 10A), fructose 1,6-bisphosphate (FBP) (Fig. 10B) and fructose 6-phosphate (F6P) (Fig. 10C) showed strong diurnal alterations, higher levels being observed at the end of the day, which is in-line with the changes in Calvin-Benson cycle activity. These diurnal changes in metabolite levels were differentially modified in the *trxf1 ntrc* mutant. Compared to wild-type, the day-time increase in the level of 3PGA, the first fixation product of Rubisco, was attenuated by 75% in the *trxf1 ntrc* mutant, while there were no changes in the *trxf1*, and only a smaller decrease (by 35%) in the *ntrc* mutant (Fig. 10A). In contrast to this, the day-time levels of FBP, the substrate of FBPase, were significantly increased by 50, 125 and 75% in *trxf1*, *ntrc* and *trxf1 ntrc* mutants, respectively (Fig. 10B), while those of F6P, the product of FBPase, were only slightly increased in *trxf1* and *ntrc* single mutants, or even decreased in the *trxf1 ntrc* double mutant, compared to wild-type (Fig. 10C). Concerning the ratio between product and substrate of FBPase (F6P/FBP), there was a significant and progressive decrease down to 80, 55 and 45% of wild-type level in *trxf1*, *ntrc* and *trxf1 ntrc* mutants, respectively (Fig. 10D), indicating a progressive inhibition of plastidial FBPase in vivo and confirming the decrease in FBPase activity and cpFBPase reduction state (Fig. 7). It should be noted that whole-leaf levels of F6P and FBP were measured, which reflect the sum of the chloroplastic and cytosolic pools, not just the chloroplastic pool. However, studies with Arabidopsis mutants show that lack of chloroplastic FBPase leads to a decrease

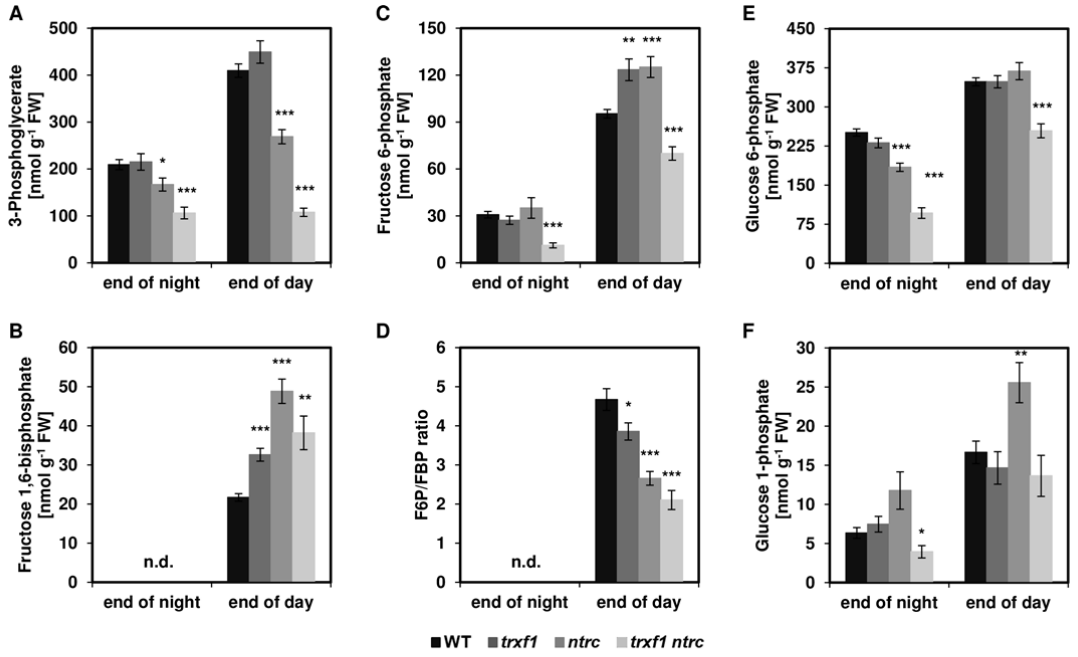

Figure 10: Changes in the in-vivo levels of phosphorylated intermediates in leaves of *trxf1*, *ntrc* and *trxf1 ntrc* Arabidopsis mutants compared to wild-type. **(A)** 3-phosphoglycerate (3PGA) level, **(B)** fructose 1,6-bisphosphate (FBP) level, **(C)** fructose 6-phosphate (F6P) level, **(D)** F6P/FBP ratio, **(E)** glucose 6-phosphate (G6P) level, and **(F)** glucose 1-phosphate (G1P) level were measured in leaves sampled at the end of the night and end of the day. Results are means ± SE, *n* = 20-30 (wild-type) or 10-15 (mutants) independent plant replicates growing in an 8 h photoperiod with 160 µmol photons m^{-2} s^{-1}. *: P<0.05, **: P<0.01, ***: P<0.001 (according to Student's *t*-test); n.d. = not detectable (values were below the detection limit)

in the overall F6P/FBP metabolite ratio, while there was no change in the F6P/FBP ratio in response to a lack of cytosolic FBPase (Rojas-Gonzalez et al. 2015). This demonstrates that a decrease in the overall F6P/FBP ratio is indicative for an inhibition of chloroplastic rather than cytosolic FBPase.

Compared to wild-type, glucose 1-phosphate (G1P), the substrate of AGPase, remained unchanged or increased slightly in the different genotypes, indicating that the inhibition of starch synthesis was unlikely to be due to a shortage of this substrate (Fig. 10F). At the end of the night, the levels of 3PGA (Fig. 10A) and hexose-phosphates (Figs. 10C, E, F) all showed a progressive decrease in *trxf1*, *ntrc* and *trxf1 ntrc* mutants relative to the wild-type, with the decrease being specifically pronounced in the *trxf1 ntrc* double mutant. This is consistent with a progressive shortage of carbon in these mutants. Nocturnal levels of FBP were below the detection limit in all genotypes (Fig. 10B).

To gain a more in-depth insight into the global effects of Trx *f*1 and NTRC on redox regulation of metabolism, GC-MS based metabolite profiling was performed. Suppl. Table S4 and Fig. 11A show significant changes in leaf metabolite levels at the end

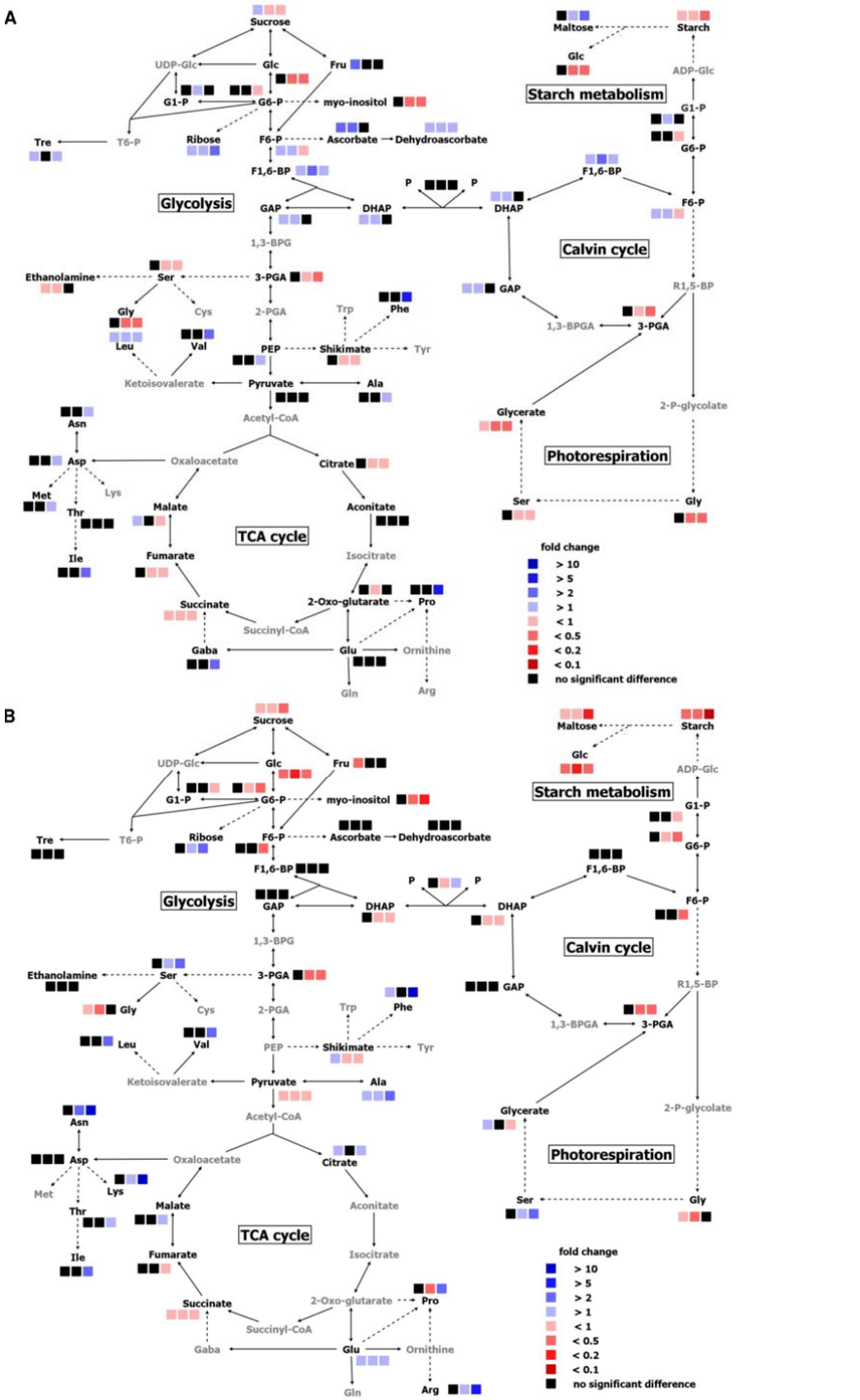

Figure 11: Overview of changes in metabolite profiles from leaves of *trxf1*, *ntrc* and *trxf1 ntrc* Arabidopsis mutants compared to wild-type. Results from leaves sampled at the end of day **(A)** and end of night **(B)** are visualized using Vanted diagrams. Metabolite levels which are significantly different from wild-type according to the student *t*-test (P<0.05) are indicated in blue (increase) or red (decrease) color, while black color indicates no significant difference from wild-type. The order of the squares from left to right is *trxf1*, *ntrc* and *trxf1 ntrc* mutants being in first, second and third position, respectively. Data are taken from Supplemental Tables S4 – S7.

of the day in *trxf1*, *ntrc* and *trxf1 ntrc* mutants, relative to the wild-type. In the *trxf1 ntrc* double mutant, sugars like glucose and raffinose decreased by a factor of 2, while the levels of maltose and ribose were 3-times and the level of trehalose 2-times increased. Similar or less strongly expressed changes in sugar levels were observed

in the *ntrc* mutant, while sugar levels remained rather unchanged or increased slightly in the *trxf1* mutant. Several organic acids showed a significant decrease in both *ntrc* and *trxf1 ntrc* mutants, such as citrate, fumarate, glycerate, 2-oxoglutarate, shikimate, succinate and threonate, while malate decreased only in the double mutant. The decrease in glycerate (3-fold), suggests possible effects on photorespiration. In contrast to this, organic acid levels were largely unchanged or showed only slight alterations in the *trxf1* mutant. Also amino acids showed large and significant alterations in the *trxf1 ntrc* mutant. With the exception of glycine and serine which were both 2-fold decreased, most other amino acids were increased in the double mutant, this is the case of alanine (1.4-fold), aspartate (1.8-fold), asparagine (2-fold), isoleucine (2.3-fold), leucine (2-fold), methionine (1.4-fold), phenylalanine (6.7-fold), proline (7.2-fold) and valine (2.2-fold). Amino acids remained unchanged or showed only slight changes in the *trxf1* and *ntrc* single mutants, with the exception of glycine and serine, which both decreased by a similar degree in the *ntrc* single and *ntrc trxf1* double mutants. The strong increase in most of the amino acids at the expense of organic acids indicates that combined deficiency of Trx *f*1 and NTRC has led to a stimulation of nitrogen assimilation, probably due to the increase in the NADP redox and adenylate energy states. The decrease in glycine and serine is consistent with combined effects on photorespiration. The strong increase in ascorbate which was observed in the *trxf1* and *ntrc* single mutants was strongly attenuated in the double mutant.

Metabolite levels were also determined at the end of the night where sugars derive from the degradation of starch reserves (Suppl. Table S5 and Fig. 11B). Compared to wild-type, *trxf1*, *ntrc* and *trxf1 ntrc* mutants showed a further progressive decrease in the levels of various sugars, with the double mutant revealing a specifically strong decrease in maltose (down to 19% of wild-type level) and sucrose (46% of wild-type level) consistent with an increased shortage of carbon under these conditions. There were significant decreases in the levels of various organic acids, which in most cases were more severe in the double mutant, compared to the single mutants, specifically fumarate, glycerate, pyruvate, shikimate and succinate. Large and significant alterations were observed in the levels of various amino acids, which increased in the double mutant, compared to wild-type or the single mutants. While glycine decreased, there were increases in the levels of alanine (3-fold), arginine (7.5-fold),

asparagine (43.7-fold), glutamate (1.9-fold), isoleucine (4-fold), leucine (3.3-fold), lysine (10.2-fold), phenylalanine (10.3-fold), proline (2.4-fold), serine (2.3-fold), threonine (2-fold) and valine (2.6-fold). The more than 10-fold increase in phenylalanine, while shikimate levels were 1.5 fold decreased, indicates aromatic amino acid synthesis to be strongly stimulated by the combined deficiency of Trx *f*1 and NTRC.

Reporter studies provide evidence for co-localization of Trx *f*1 and NTRC in the same chloroplast sub-structure and in the same tissues

The above data clearly show combined functions of Trx *f*1 and NTRC in regulating photosynthetic metabolism. To investigate whether this is accompanied by a possible co-localisation of Trx *f*1 and NTRC, we analyzed the subcellular localization pattern of the two proteins. Constructs were generated, containing the full length cDNA of Trx *f*1 fused to YFP and NTRC fused to cyan fluorescent protein (CFP), respectively. Pairwise expression of these fusion proteins in *Nicotiana benthamiana* leaves resulted in YFP and CFP fluorescence signals which were induced in discrete regions inside the chloroplast (Fig. 12). As revealed by the merged picture, Trx*f*1:YFP and NTRC:CFP fluorescence pattern were congruent to each other, indicating that both Trx *f*1 and NTRC co-localized in the same sub-chloroplast structure (Fig. 12). We also analyzed the expression pattern of Trx *f*1 at the tissue level. GUS analysis of Trx *f*1 expression (Suppl. Figure S2) reveals a pattern similar to NTRC expression in Arabidopsis plants (Kirchsteiger et al., 2012). This indicates that Trx *f*1 and NTRC are both active in the same tissues, highlighting the biological relevance of their cooperative function.

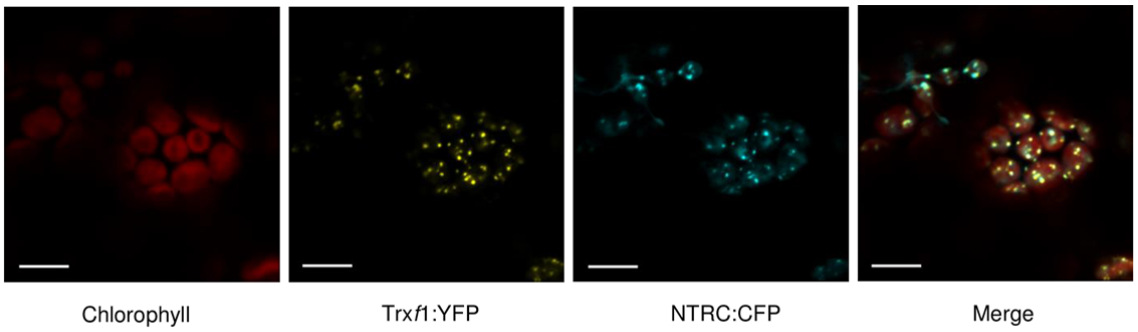

Figure 12: Suborganellar localization of Trx *f*1 and NTRC proteins. Co-localization of Trx*f*1:YFP and NTRC:CFP fusions in transiently transformed leaf mesophyll cells of *Nicotiana benthamiana*. The red auto-fluorescence of chlorophyll, yellow fluorescence of YFP, blue fluorescence of CFP and the merge of the three fluorescent images are shown from left to right. Pictures were monitored in the channel mode with identical microscope settings. Bars = 10 µm

DISCUSSION

Two different thiol redox-systems exist in plant chloroplasts, the Fdx-Trx, which is dependent of Fdx reduced by the photosynthetic electron transport chain and, thus, of light, and the NADPH-NTRC system, which relies on NADPH and thus may be operative also during the night. Previous studies led to the view that the two different systems may have different functions in plants. However, the possibility remains that both systems might act cooperatively. In the present work we have tested this possibility by using a genetic approach. Results provide evidence that light and NADPH dependent redox systems interact at the level of Trx *f*1 and NTRC to coordinately participate in the regulation of photosynthetic carbon metabolism and growth in response to changes in light conditions.

Trx *f*1 and NTRC cooperatively participate in light regulation of the Calvin-Benson cycle and growth while having no effect on the redox regulation of the malate valve

Our results show that single knockouts of Trx *f*1 or NTRC cause no or only slight impairment of photosynthesis (Fig. 3 and 4), respectively, confirming previous studies (Lepisto et al., 2009; Thormählen et al., 2013). Interestingly, the combined deficiency of both thiol redox-regulators led to a more severe inhibition of photosynthetic CO_2-assimilation (Fig. 3), electron transport rates (Fig. 4) and growth (Fig. 2) than in both single knockouts. This was accompanied by an increase in both the NADPH/$NADP^+$

642 and ATP/ADP ratios (Fig. 6), indicating that the primary cause for the strong
643 impairment of photosynthesis is an inhibition of the Calvin-Benson cycle rather than
644 the light reactions. Direct measurements of FBPase, a key enzyme of the Calvin-
645 Benson cycle, confirm this interpretation (Fig. 7). Light activation of FBPase was
646 attenuated by up to 50% in the Trx *f*1 and NTRC single mutants, while it was almost
647 completely abolished in the double mutant. A similar picture emerged when the
648 redox-state of the regulatory disulfide of chloroplast FBPase was directly analyzed
649 using gel-shift assays in vivo. Inhibition of FBPase is also indicated at the metabolite
650 level, since it was accompanied by a decrease in F6P/FBP metabolite ratios in-vivo
651 (Fig. 10D). This shows that combined knockout of Trx *f*1 and NTRC strongly impedes
652 light-dependent changes in FBPase redox transition (Fig. 7) and hence Calvin-
653 Benson cycle activity (Fig. 3) and plant growth (Fig. 2). Results are in-line with
654 previous studies on transgenic plants (Koßmann et al., 1994) or Arabidopsis mutants
655 (Livingston et al., 2010; Rojas-Gonzalez et al. 2015) with knock-down of chloroplast
656 FBPase showing that a decrease in chloroplast FBPase activity below 36% of wild-
657 type level impairs F6P/FBP metabolite ratios, photosynthetic CO_2 assimilation, starch
658 accumulation and growth.
659
660 In textbooks, Trx *f* is proposed to act as the exclusive thiol redox-regulator of FBPase
661 and the Calvin-Benson cycle, a scenario which is based on pioneering in-vitro
662 experiments of Buchanan and coworkers back in the seventies (Buchanan et al.,
663 1979; Buchanan, 1980) and subsequent comparative studies using a large set of
664 different recombinant purified Trx isoforms in vitro (Collin et al. 2003). Our in-vivo
665 studies show that this textbook view cannot be transferred to the more complex
666 situation in planta, where an almost complete deficiency of Trx *f* has been found to be
667 not sufficient enough to decrease light dependent redox activation of FBPase by
668 more than 50% (compare Fig. 1 and Fig. 7). The latter requires a combined
669 deficiency of Trx *f* and NTRC, indicating that both proteins have redundant functions
670 in light-regulation of FBPase and the Calvin-Benson cycle activity in planta. The
671 involvement of NTRC in redox-regulation of the Calvin-Benson cycle allows carbon
672 assimilation to be linked to the NADP redox state as an additional input, which is
673 influenced by light via FNR and by metabolic parameters.
674

In contrast to the strong effects on FBPase, single and combined knockouts of Trx *f*1 and NTRC did not lead to any inhibition in the redox-activation of NADP-MDH (Fig. 8), a key enzyme in the export of excess reducing equivalents from the chloroplast to the cytosol via the malate valve (Scheibe, 2004). This indicates that neither Trx *f*1 nor NTRC affect NADP-MDH redox activation in planta, suggesting that the latter is regulated by other Trx isoforms, such as *m*-type Trxs. This regulatory feature could be important to prevent an imbalance of the chloroplast NADP redox state. If Trx *f*1 and NTRC would activate Calvin-Benson cycle and the malate valve simultaneously, this could lead to a strong depletion in chloroplast NADPH levels with adverse effects on the operation of the Calvin-Benson cycle. Our results therefore show that the predominant role of Trx *f* in redox regulation of NADP-MDH which was proposed on the basis of in-vitro studies (Collin et al. 2003; Yoshida et al. 2015) cannot be translated to the situation in planta.

Trx *f*1 and NTRC cooperatively participate in light regulation of starch metabolism and balancing of carbon and nitrogen metabolism

Combined deficiency of Trx *f*1 and NTRC led to a nearly complete inhibition of starch accumulation. This was accompanied by an additive decrease in light activation of the key enzyme of starch synthesis, AGPase (Fig. 9). The effect is most likely attributable to both Trx *f*1 and NTRC being able to reduce the small subunit of AGPase with similar efficiencies, as observed by previous in-vitro studies (Thormählen et al., 2013). In the *trxf1 ntrc* double mutant, the additive decrease in redox-activation of AGPase will partly contribute to the strong decrease in starch accumulation (compare Figs. 9A and 9D), while there will be an additional contribution from the inhibition of the Calvin-Benson cycle (Fig. 3A) and the subsequent decrease in the level of its first fixation product 3PGA (Fig. 10A), which is a strong allosteric activator of AGPase (Preiss 1988). Changes in the redox (Hädrich et al. 2012) and allosteric properties of AGPase (Obana et al. 2006; Mugford et al. 2014) have been found to substantially alter diurnal starch turnover in leaves of Arabidopsis plants.

Interestingly, combined - but not single - deficiencies of Trx *f*1 and NTRC led to a strong and unexpected increase in the level of the starch degradation product

maltose during the light period (Fig. 11A and Table 1). This could indicate that Trx *f*1 and NTRC may participate in the diurnal regulation of starch degradation in addition to starch synthesis. This is in-line to previous in-vitro studies reporting that several enzymes in the pathway of starch degradation are subject to thiol redox-regulation (Valerio et al., 2011; Glaring et al., 2012), including a plastid-targeted beta-amylase which has been shown to be regulated by both Trx *f*1 and NTRC (Valerio et al., 2011). It remains to be determined whether a similar mechanism is operational in vivo.

Unexpectedly, combined deletion of Trx *f*1 and NTRC resulted in a strong increase in the levels of most amino acids, while sugars and organic acids were mainly decreased (Fig. 11), indicating an induction of nitrogen assimilation in the face of a decreased carbon assimilation. It is unlikely that this is due to direct effects of Trx *f*1 and NTRC deficiencies on redox-activation of enzymes involved in nitrogen assimilation, such as nitrate and nitrite reductase, glutamate:oxoglutarate aminotransferase or glutamine synthetase, since this would have led to a decrease rather than an increase in the activities of theses enzymes (Lichter und Häberlein 1998; Choi et al. 1999). However, there will be indirect effects due to the elevated NAD and NADP reduction and adenylate energy states as a consequence of the inhibition of carbon assimilation (Fig. 6), which will promote nitrogen assimilation by increasing the levels of its cofactors. This is accompanied by a decrease in the levels of organic acids, which are used as substrates to provide carbon skeletons for amino acid synthesis. These results suggest a combined role of Trx *f*1 and NTRC in balancing carbon and nitrogen assimilation as well as the levels of sugars and amino acids to avoid an over-reduction of PS I and osmotic imbalances, respectively (Fernie et al., 2002; Faix et al., 2012). Alternatively, the increase in amino acids may also be attributable to (i) the overall attenuation of protein synthesis in the cell because of the strongly reduced growth rate of the double mutant, or (ii) a specific stimulation of protein degradation to mobilize additional carbon reserves when sugars are limiting. However, in both of these scenarios, organic acid levels would increase rather than decrease.

Trx *f*1 and NTRC cooperatively participate in light acclimation of photosystem I

743 Impaired photosynthetic light reactions in the *trxf1 ntrc* mutant were most likely a
744 consequence of the inhibition of the Calvin-Benson cycle and the subsequent
745 increase in NADPH/$NADP^+$ ratios (Figs. 4, 3 and 6B). Combined knockout of Trx *f*1
746 and NTRC led to a strong decrease in the abundance of PSI core proteins (Fig. 5),
747 which was most likely due to an inhibition of electron transfer at the acceptor side of
748 PSI, leading to its over-reduction. As shown by previous studies, PSI is very sensitive
749 to excess electrons delivered from PSII due to its limited capacity of regeneration by
750 protein turnover (Suorsa et al., 2012; Tikkanen and Aro, 2014). The moderate
751 decreases in the abundance of PSII core proteins (Fig. 5) and in chlorophyll levels
752 (Suppl. Fig. S1) are most likely part of an adaptive response to relieve the electron
753 pressure on PSI and to protect PSI from photo-damage (Grieco et al., 2012; Suorsa
754 et al., 2012; Tikkanen et al., 2014). The decreased ability of the *trxf1 ntrc* mutant to
755 adapt to high-light conditions (Fig. 2F) provides further evidence for a role of Trx *f*1
756 and NTRC in light-acclimation of PSI. Proteins involved in cyclic electron transport
757 around PSI may also be part of an adaptive response to preserve PSI, although their
758 specific functions remain to be clarified (Livingston et al., 2010; Suorsa et al., 2012;
759 Hertle et al., 2013). Interestingly, an Arabidopsis mutant deficient in chloroplast
760 FBPase showed impaired linear electron transport and increased cyclic electron flow
761 (Livingston et al., 2010). More studies are needed to resolve the roles of the stromal
762 redox-regulators Trx *f*1 and NTRC in the regulatory network of plant thylakoid energy
763 transduction.
764
765 Alternatively, our data could indicate more specific effects of Trx *f*1 and NTRC on
766 chloroplast protein synthesis. It has been shown in previous studies that light plays a
767 crucial role in regulating chloroplast protein translation, which most likely involves the
768 Fdx-Trx system as one of the underlying signaling pathways (Pfannschmidt and
769 Liere, 2005). More recently, a role of NTRC was proposed to regulate translation of
770 the D2 protein of PSII by thiol-disulfide modulation of chloroplast translation factors in
771 *Chlamydomonas reinhardtii* (Schwarz et al., 2012). However, in-vivo evidence to
772 support this conclusion is lacking at the moment.
773
774 **Trx *f*1 and NTRC cooperatively participate in growth acclimation to varying**
775 **light conditions**
776

Combined - but not single - deficiencies of Trx *f*1 and NTRC severely affected growth acclimation to varying light conditions, leading to strongly impaired acclimation of plant growth to a decrease in the length of the photoperiod or changes in light intensities over a wide range of conditions (Fig. 2H). The ability to acclimate to a 4 h photoperiod or to low light intensity (30 µmol photons m^{-2} s^{-1}) was almost completely lost, as well as the ability to acclimate to high-light conditions (950 µmol m^{-2} s^{-1}). The vulnerability of the *trxf1 ntrc* double mutant to low light conditions is most likely due to its strongly impaired ability to activate the Calvin-Benson cycle in response to light. Decreased photoperiods but also low light intensities require efficient mechanisms to fully activate the Calvin-Benson cycle when light becomes available. The decreased ability of the *trxf1 ntrc* double mutant to acclimate to high light is most likely attributable to the increased sensitivity of PSI to photo-damage (see Fig. 5 and discussion above). The strong depletion in soluble sugars prevailing in the double mutant (Fig. 11) may also have contributed to the decrease in its ability for high-light acclimation. As shown in previous studies, soluble sugars act as signals in the high-light response of Arabidopsis plants, while high-light acclimation is impaired when soluble sugar levels are decreased (Schmitz et al., 2014). Overall, these results suggest a combined role of Trx *f*1 and NTRC in growth acclimation to varying light conditions.

Trx *f*1 and NTRC co-localize in the same chloroplast substructure

The Trx*f*1:YFP and NTRC:CFP fusion proteins were found to be co-localized in discrete regions within the chloroplast stroma (Fig. 12). The pattern is similar to that previously reported for the interaction of NTRC with 2-Cys Prx (Bernald-Bayard et al. 2014) or the CHL-1 subunit of the Mg-chelatase complex (Perez-Ruiz et al. 2014) and for immunogold-labelling of NTRC (Perez-Ruiz et al. 2009). The co-localization of these clusters with specific chloroplast structures is not clear from these studies. Our preliminary results indicate that the substructure where Trx *f*1 and NTRC are co-localized does not correlate with chloroplast nucleoids, but was found to be associated to starch granules (data not shown). The vicinity of these clusters to starch granules may be related to the combined function of Trx *f*1 and NTRC in regulating carbon assimilation and storage.

MATERIALS AND METHODS

Plant material and growth conditions

Arabidopsis thaliana T-DNA insertion lines *trx f1* (SALK_128365; Thormählen et al., 2013), *ntrc* (SALK_012208; Perez-Ruiz et al., 2006), the double mutant *trxf1 ntrc*, generated by cross breeding, and the respective Col-0 wild-types were grown for five weeks on potting soil (Stender, Germany) in a growth chamber with 8 h photoperiod, 160 µmol photons m^{-2} s^{-1}, 20°C/16°C, and 60%/75% humidity (day/night), if not indicated otherwise in the figure legends. For rosette fresh-weight determination, plants were grown for the first week under the conditions indicated above, before they were transferred to 16 h or 24 h photoperiods for additional 3 weeks or to 4 h photoperiod, 30 or 950 µmol photons m^{-2} s^{-1} for additional 4 weeks using a growth chamber at 21°C.

Homogenisation of plant material

For all the metabolite, DNA or protein extractions described below, leaves were shock-frozen directly into liquid nitrogen, and subsequently homogenized to a fine powder using a liquid nitrogen-cooled ball mill (MM 400, Retsch GmbH, Haan, Germany).

Selection and molecular characterization of the knockout lines

The *trxf1 ntrc* mutant was selected after crossing the well-characterized homozygous parental lines carrying T-DNA insertions in *Trx f1* (Thormählen et al., 2013) and *NTRC* genes (Perez-Ruiz et al., 2006). The selection of a homozygous line with insertion in both alleles was performed by PCR analyses of genomic DNA using gene-specific primers for the *Trx f*1 (At3g02730; 5`-TGTCAGTGTTGGTCAGGTGAC-3` and 5`-AGAACCCATCCAACACACTTG-3`) and *NTRC* (At2g41680; 5`-TATTGAGCAACACCAAGGGAC-3` and 5`-CATAATTCCAGCTGCTTCAGC-3`) genes or oligonucleotides of the T-DNA (5´-ATTTTGCCGATTTCGGAAC-3`). PCR products were fractionated on 1 % agarose gels, and visualized by ethidium bromide staining. Detection of Trx *f* and NTRC proteins was done by Western blot analysis

(Laemmli, 1970) using antibodies raised against pea Trx *f* (Hodges et al., 1994) and rice NTRC (Serrato et al., 2004). To do this, frozen leaf powder was extracted with 2-fold Laemmli buffer (Laemmli, 1970) including 20 mM DTT instead of β-mercaptoethanol. After shaking the extract for 3 min at 90°C, each lane of the polyacrylamide gels was loaded with sample corresponding to 1 mg fresh weight for each genotype. The pea Trx-*f* antibody used in these experiments has been found in previous studies to recognize Arabidopsis Trx *f*1 and Trx *f*2 recombinant proteins with comparable efficiencies (Thormählen et al., 2013).

Gas exchange measurements

Photosynthesis-related gas exchange parameters were determined on 4 to 5 week old plants with the portable GFS-3000 system (Heinz Walz GmbH, Effeltrich, Germany). The control unit 3000-C with the measuring head 3010-S was used by adapting the cuvette to Arabidopsis Chamber 3010-A. The conditions within the cuvette were 22°C, 60% relative humidity and ambient CO_2 concentrations, while the impeller speed was set to 7, and the flow rate to 750 µmol s^{-1}. The monitoring of the light curve was started with darkened rosettes. When the CO_2 and H_2O system parameters were stabilized, the light was switched on and changed in the following order: 50, 100, 150, 200, 300, 400, 600, 800, 1000 µmol m^{-2} s^{-1}. The parameters of CO_2 assimilation rate, transpiration rate and intercellular CO_2 mole fraction were calculated by the software GFS-Win V3.50b (Heinz Walz GmbH, Effeltrich, Germany).

Chlorophyll fluorescence analysis

For the in vivo chlorophyll a fluorescence measurement and the calculation of standard photosynthesis parameters of PSII, a Dual PAM fluorometer (Dual-PAM 100, Walz GmbH, Effeltrich, Germany) was used as described previously (Thormählen et al., 2013).

Analysis of chlorophyll content

878 The chlorophyll level was determined and calculated as described in Porra et al.
879 (1989). 25 mg frozen leaf material was extracted twice with 1 ml 80% acetone. For
880 each extraction step the samples were vortexed for two minutes, incubated for 10
881 min in darkness on ice, and 10 min centrifuged at 4°C. The collected supernatants
882 were pooled, and the light absorption measured at 663 nm, 645 nm, and 750 nm
883 (absorption at 750 nm was substracted from the values at 665 nm and 652 nm) with
884 an UV/VIS spectrophotometer (Ultrospec 3100 pro, GE Healthcare Europe GmbH,
885 Freiburg, Germany).
886
887 **Enzyme-coupled analysis of metabolite levels by spectrophotometry**
888
889 For metabolite analysis, leaf samples were directly frozen in liquid nitrogen without
890 any shading allowing rapid quenching of metabolism. Extraction and analysis of the
891 pyridine nucleotides NAD, NADP, NADH and NADPH were performed as described
892 previously (Lintala et al., 2014). In brief, 25 mg frozen leaf powder was resuspended
893 in 250 µl 0.1 M $HClO_4$ (NAD^+ and $NADP^+$) or 250 µl 0.1 M KOH (for NADH and
894 NADPH, respectively) and incubated for 10 min on ice. Samples were centrifuged at
895 20,000 *g* for 10 min at 4°C and the supernatant was heated to 95°C for 2 min. The
896 pH was adjusted to 8.0 – 8.5 by addition of an equal volume 0.2 M Tris (pH 8.4), 0.1
897 M KOH or 0.2 M Tris (pH 8.4), 0.1 M HClO4, respectively. The final detection mix for
898 NAD(H) contained 100 mM Tricine/KOH (pH 9), 4 mM EDTA, 500 mM EtOH, 0.1 mM
899 phenazine ethosulfate (PES), 0.6 mM methylthiazolyldiphenyl-tetrazolium bromide
900 (MTT), 6 U ml^{-1} alcohol dehydrogenase (ADH). For NADP(H) the final mix consisted
901 of 100 mM Tricine/KOH (pH 9), 4 mM EDTA, 3 mM glucose 6-phosphate, 0.1 mM
902 PES, 0.6 mM MTT and 6 U ml^{-1} G6PDH. Absorption was monitored at 570 nm at
903 30°C in a microplate reader (HT3, Anthos Mikrosysteme GmbH,
904 http://www.anthos.de/). To validate the method, small representative amounts (two to
905 threefold the endogenous content) of NAD^+, $NADP^+$, NADH and NADPH were added
906 to the plant material in the killing mixture of $HClO_4$ or KOH. The recoveries of these
907 metabolites from Arabidopsis leaves during extraction and assay were (as
908 percentage of the amount added): NAD^+, 92 %; $NADP^+$, 98 %; NADH, 79 % and
909 NADPH, 111 %. The extraction of ATP and ADP was performed according to
910 previous studies, where also the validity of this method has been documented (Jelitto
911 et al., 1992). In brief, 50 mg frozen leaf powder was extracted with ice-cold 16% TCA

(w/v), 5 mM EGTA by vortexing 1 h at 4°C. After centrifugation for 10 min at 4°C with 20,000 *g*, the supernatant was shortly mixed with 4 ml ice-cold, water-saturated diethyl ether (DEE) and centrifuged again at 3,200 *g* at 4°C for 5 min. The upper ether phase was discarded to repeat the washing step. The pH adjustment of the remaining water phase was done with 5 M KOH, 1 M triethanolamine or 1 M HCl until a pH of 6-7 was reached. The remaining DEE in the extract evaporated under the hood for 1 h on ice. Directly after the extraction, ATP and ADP levels were measured enzymatically as described previously (Stitt et al., 1989), with the exception that the change in NAD(P)H levels was measured by fluorescence spectroscopy in 96-well micro plates at 360 nm with a FilterMax F5 Multi-Mode Microplate reader (Molecular Devices, Sunnyvale, USA). Starch and sucrose were measured photometrically by NADPH absorption, hexose phosphates, FBP, triose phosphates and 3PGA by NAD(P)H fluorescence as described previously (Thormählen et al., 2013). Each individual plant sample was measured with at least 2 analytical replicates.

GC-TOFMS analysis of polar primary metabolites

GC-TOFMS-based analysis of primary metabolites was performed exactly as described previously (Thormählen et al., 2013). For each biological replicate three analytical replicates were measured. To visualize the metabolite changes within an overview, we used the open source software VANTED version 2.1.0 (http://vanted.ipk-gatersleben.de/).

Immunodetection of photosynthesis and starch related proteins

Proteins involved in photosynthetic electron transport (PsaA, PsaB, PsbA, PsbD, Lhca1, Lhcb1, PetC, Atpβ), Rubisco (RbcL) and actin were detected by Western blotting using specific antibodies (Agrisera, Vännäs, Sweden) according to company instructions. Frozen leaf powder was extracted with 2-fold Laemmli buffer (Laemmli, 1970) including 20 mM DTT instead of β-mercaptoethanol. After shaking the extract for 3 min at 90°C, each lane of the polyacrylamide gels was loaded with sample corresponding to 1 mg fresh weight (100%) for each genotype. Immunoblotting of APS1, detection and quantification of ECL signals were performed as described previously (Thormählen et al., 2013).

946

947 **FBPase gel-shift assays**

948

949 For FBPase gel-shift assays proteins from leaves of wild-type and mutant plants,
950 harvested at the end of the night (EN) or the day (ED), were extracted in the
951 presence of 10% (v/v) trichloroacetic acid (TCA) and protein thiols were alkylated
952 with 10 mM MM(PEG)$_{24}$. For the Western blot analysis, samples were subjected to
953 SDS-PAGE (9.5% polyacrylamide) under non-reducing conditions, transferred onto
954 nitrocellulose membranes and probed with an anti-FBPase antibody kindly provided
955 by Mariam Sahrawy (Estación Experimental del Zaidín, CSIC, Granada, Spain).
956 Quantification of the protein band intensities was done by using the open source
957 software ImageJ version 1.49g (http://imagej.nih.gov/ij/).

958

959 **Enzyme activity measurements**

960

961 The activity of plastidial FBPase was determined as described in a previous study
962 (Holaday et al., 1992). In short, 20 mg frozen leaf powder was rapidly extracted with
963 1 ml ice-cold extraction buffer (10 mM $MgCl_2$, 1 mM EDTA, 0.05 % [v/v] Triton X-100,
964 100 mM Tris [pH 8, HCl], 1 mM fructose 1,6-bisphosphate) and centrifuged with
965 18.000 *g* at 4°C. 10 µl of the supernatant was added immediately to 190 µl assay
966 mixture in the well of 96-well microplate. The final assay contained 10 mM $MgCl_2$, 1
967 mM EDTA, 0.05 % Triton X-100, 100 mM Tris (pH8, HCl), 0.5 mM $NADP^+$, 2 units ml^{-1}
968 G6PDH and 4 units ml^{-1} PGI. For the maximal activity measurement, 10 mM DTT
969 was included in the assay. To start the reaction, FBP (0.1 mM for initial activity and 4
970 mM for the maximal activity) was added, while NADPH formation was measured
971 spectro-photometrically at 340 nm using a micro-plate reader (HT-3, Anthos
972 Mikrosysteme GmbH, Krefeld, Germany). The activity of NADP-malate
973 dehydrogenase was measured as described previously (Lintala et al., 2014). Every
974 individual plant sample was measured with at least 2 analytical replicates.

975

976 **Subcellular localization studies**

977

978 For co-localisation studies of NTRC and Trx *f*1 the entire coding region of each gene
979 was amplified from Arabidopsis (Col-0) cDNA by PCR using the following primer

pairs (NTRC-fwd 5´-CACCATGGCTGCGTCTCCCAAGATAGGCATCGGTAT-3´/NTRC-rev 5`-TTTATTGGCCTCAATGAATTCTCGGTACTCTTT-3` and Trxf1-fwd 5´-CACCATGCCTCTTTCTCTCCGTCTTTCTCCTTCGCC-3/TRXf1-rev 5´-TCCGGAAGCAGCAGACTTCGCTGTTTCAATCGC-3´). The PCR products were inserted into the pENTR-D/TOPO (Invitrogen) entry vector and were checked by sequencing. Trx *f1* and NTRC entry vectors were used to generate C-terminal fusion gene constructs with full length YFP and CFP, respectively. As destination vectors, the GATEWAY-compatible 35S::Venus-pBar and 35S::sCFP3A-pBar were used (Zakharov et al., 2004). Each binary vector construct was separately transformed into *Agrobacterium tumefaciens* strain EHA105 for subsequent transient transformation of leaves of 4 week-old *Nicotiana benthamiana* grown in soil under greenhouse conditions. Specific fluorescence signals were monitored by Zeiss LSM 780 confocal laser scanning microscope 48 h after combined infiltration of the different gene fusion constructs into tobacco leaves. Fluorophore signals, chlorophyll autofluorescence and bright field images were scanned sequentially in channel mode to prevent any crosstalk between fluorescence channels. The lambda mode was used to confirm the spectral signature of the fluorophores.

Promoter-GUS analysis

An 875 bp fragment of the *Trx f1* gene promoter was amplified from Arabidopsis (Col-0) DNA by standard PCR method using a Phusion DNA polymerase (Thermo Scientific) and the following primer pair (Tf1prom-fwd 5´-TACTGCAGGCGGTGGAGTACGATTTAGGACAAAGAA-3´/Tf1prom-rev 5´-TAGTCGACTGTTTGAGGAATTCAACAGAGAGACGAT-3´). The PCR product was restricted with *Pst*I and *Sal*I (Thermo Scientific) and cloned into the pBAR binary vector (Zakharov et al., 2004) containing the GUS-reporter expression cassette. The construct was transformed into cells of the *Escherichia coli* DH5α strain for amplification and subsequent sequencing of the plasmids. Purified plasmids were used for *Agrobacterium tumefaciens* mediated transformation of *Arabidopsis thaliana* (Col-0) via the floral dip method (Clough and Bent, 1998). Transformed plants were selected for homozygosity and assayed for GUS activity as described previously (Jefferson et al., 1987). GUS stained specimens were bleached in 70% (v/v) ethanol and either directly analyzed by stereomicroscopy (Zeiss Stereo Lumar.V12) or

samples were cleared by mounting in Hoyer´s solution (100 g chloral hydrate, 5 ml glycerol in 30 ml water). Cleared specimens were imaged by differential interference contrast microscopy (Zeiss Axio Imager.M2).

Statistical Analysis

The statistical data analyses were done with Microsoft Office Excel 2007 (Student's *t*-test) and SYSTAT Sigma Plot 11 (two way analysis of variance, Tukey´s multiple comparison test). The Student´s *t*-test was done as a two-tailed test assuming unequal or equal variance depending on the data (checked by performing an F-test in the beginning). When Western blot signals were quantified, the paired *t*-test was used.

ACKNOWLEDGEMENTS

We are grateful to Anne Orwat (LMU Munich) for excellent technical assistance, Ana Luz Rodriguez Muslera (LMU Munich) for performing preliminary work, Dario Leister (LMU Munich) for providing facilities for PAM analysis and a set of antibodies to analyze photosynthetic proteins, Jürgen Soll (LMU Munich) for providing facilities for gas exchange measurement, and to Emmanuelle Issakidis-Bourguet (University Paris-Orsay, France) and Mariam Sahrawy (CSIC, Spain) for providing anti-Trx *f* and anti-FBPase antibodies, respectively.

LIST OF AUTHOR CONTRIBUTIONS

I.T., T.M. and P.G. designed research. I.T., T.M, J.G. A.B.Ö., E.v.R.-L., B.N. and F.J.C. performed research. I.T., T.M, J.G. A.B.Ö., E.v.R.-L., B.N., F.J.C. and P.G. analyzed data. I.T., T.M., F.J.C. and P.G. wrote the article.

FIGURE LEGENDS

Figure 1: Molecular characterization of *trxf1*, *ntrc* and *trxf1 ntrc* Arabidopsis mutants compared to wild-type. **(A)** Genotyping by PCR analysis with different primer combinations (wild-type or insertion) for the identification of T-DNA insertions in *Trx f1* and *NTRC* genes. **(B)** Detection of Trx *f* and NTRC proteins using Western blot analysis. Representative Western blots are shown of measurements, which were performed in leaves of 5-week old plants grown in an 8h-day with 160 µmol photons m^{-2} s^{-1} light regime harvested 4 h into the light period. Rubisco protein level is shown as control.

Figure 2: Growth analysis of wild-type, *trxf1*, *ntrc* and *trxf1 ntrc* Arabidopsis mutants across different light conditions. **(A)**, **(B)**, **(E)** and **(F)** correspond to 5 week-old plants, while **(C)** and **(D)** correspond to 4 week-old plants, and **(G)** to 7 week-old plants. In the first week, plants - except (**G**) - were grown in an 8 h-day and moderate light intensity regime before they were transferred for additional 3-4 weeks to the conditions indicated below: **(A)** 4 h-day and moderate light intensity , **(B)** 8 h-day and moderate light intensity, **(C)** 16 h-day and moderate light intensity, **(D)** 24 h-day and moderate light intensity, **(E)** 8 h-day and low light intensity, **(F)** 8 h-day and high light intensity, and **(G)** 16 h-day in greenhouse. In **(H)**, rosette fresh-weights of plants corresponding to the conditions shown in **(A)** to **(F)** are given as percent of wild-type levels in the respective conditions. Results are the mean ± SE, *n* = 30-86 (wild-type), 15-44 (*trxf1*), 5-44 (*ntrc*) or 9-111 (*trxf1 ntrc*) different plants. All values are significantly different from wild-type according to the Student's *t*-test ($P<0.05$), except the *trxf1* mutant in 8 h-, 16 h- and 24 h-day regimes at moderate and high light intensities (see Suppl. Table S1). Low light intensity = 30 µmol photons m^{-2} s^{-1}; moderate light intensity = 160 µmol photons m^{-2} s^{-1}; high light intensity = 950 µmol photons m^{-2} s^{-1}; n.d. = not detectable (fresh-weight values were below the detection limit)

Figure 3: Changes in gas-exchange parameters in leaves of *trxf1*, *ntrc* and *trxf1 ntrc* Arabidopsis mutants compared to wild-type. **(A)** CO_2 assimilation rate, **(B)** transpiration rate, and **(C)** intercellular CO_2 concentration were measured at different light intensities in leaves from plants growing in an 8 h photoperiod with 160 µmol

photons m^{-2} s^{-1}. Results are the mean ± SE, *n* = 10 (wild-type) or 5 (mutants) different plant replicates. *: P<0.05, **: P<0.01, ***: P<0.001 (according to two-way analysis of variance [Anova)], Tukey test); for further statistical analysis see Suppl. Table S2; PAR = photosynthetic active radiation

Figure 4: Changes in chlorophyll fluorescence parameters in leaves of *trxf1*, *ntrc* and *trxf1 ntrc* Arabidopsis mutants compared to wild-type. Plants growing in an 8 h photoperiod with 160 µmol photons m^{-2} s^{-1} were dark adapted for 10 min, before exposure of a far red light saturation pulse (5,000 µmol m^{-2} s^{-1} for 0.8 s) to single leaves. Afterwards the maximal chlorophyll a fluorescence was quenched by electron transport with an actinic red light of 166 µmol photons m^{-2} s^{-1}. Within 10 min the steady state was reached and another saturation pulse was given. In the end, **(A)** the maximal PSII (F_v/F_m), and **(B)** the effective PSII (Φ_{PSII}), the non-regulated energy dissipation (Φ_{NO}) and the regulated energy dissipation (Φ_{NPQ}) quantum yields were calculated. Results are means ± SE, *n* = 11 different plants.
*: P<0.05, **: P<0.01, ***: P<0.001 (according to Student's *t*-test)

Figure 5: Changes in the levels of proteins involved in photosynthetic electron transport and ATP synthesis in leaves of *trxf1*, *ntrc* and *trxf1 ntrc* Arabidopsis mutants compared to wild-type. PsaA, PsaB, PsbA, PsbD, PetC, Lhca1, Lhcb1 and Atpß proteins were detected using specific antibodies. Representative Western blots are shown from 5-week old plants growing in an 8h-day with 160 µmol photons m^{-2} s^{-1} light regime harvested 4 h into the light period. In the wild-type, different amounts of samples were loaded (25-100%) for comparison. Actin protein level is shown as control.

Figure 6: Changes in nucleotide levels in leaves of *trxf1*, *ntrc* and *trxf1 ntrc* Arabidopsis mutants compared to wild-type. **(A)** Sum of NADPH and NADP, **(B)** NADPH/NADP ratio, **(C)** sum of NADH and NAD, **(D)** NADH/NAD ratio, **(E)** sum of ATP and ADP, and **(F)** ATP/ADP ratio were measured in leaves harvested at the end of day and end of night. Results are means ± SE, *n* = 20-30 (wild-type) or 10-15 (mutants) independent plant replicates. Plants were grown in an 8 h photoperiod with 160 µmol photons m^{-2} s^{-1}. *: P<0.05, **: P<0.01, ***: P<0.001 (according to Student's *t*-test).

Figure 7: Light-dependent redox activation of fructose-1,6-bisphosphatase (FBPase) in leaves of *trxf1*, *ntrc* and *trxf1 ntrc* Arabidopsis mutants compared to wild-type. **(A)** and **(B)** show the thiol-disulfide reduction state of chloroplast FBPase in leaves harvested at the end of night (EN) and end of day (ED) analyzed by using gel-shift assays: **(A)** Representative gel-shift blot using an antibody specific for chloroplast FBPase, and **(B)** calculated ratio of reduced to oxidized FBPase. **(C)** Corresponding initial enzyme activity of FBPase (assay without DTT) in leaves harvested at the end of night (EN) and end of day (ED). **(D)** to **(F)** Transient light activation of FBPase during a detailed time course. At the end of the night (0 min), plants were illuminated for different time-periods (2, 5, 10, 20 and 30 min) to measure FBPase activity using different assay conditions: **(D)** Initial activity without DTT additions in the assay, **(E)** maximal activity with 10 mM DTT included in the assay, and **(F)** estimated redox-activation state (initial/maximal activity*100). Results are means ± SE, *n* = 8 (wild-type) or 4 (mutants) independent plant replicates **(B)**, *n* = 20 (wild-type) or 10 (mutants) independent plant replicates **(C)**, and *n* = 10 (wild-type) or 4-6 (mutants) independent plant replicates **(D)** to **(F)**. All plants were grown in an 8 h photoperiod with 160 µmol photons m^{-2} s^{-1}. *: P<0.05, **: P<0.01, ***: P<0.001, according to Student's *t*-test **(B)** and **(C)** or two-way analysis of variance [Anova] Tukey test **(D)** to **(F)**, see Suppl Table S3**.** Estimation of the redox-activation state from enzyme assays **(F)** and the directly measured thiol-disulfide state of the protein **(B)** yielded different absolute values, which is most likely due to additional factors affecting FBPase activity during the enzyme assays.

Figure 8: Light-dependent redox activation of NADP-dependent malate dehydrogenase (MDH) in leaves of *trxf1*, *ntrc* and *trxf1 ntrc* Arabidopsis mutants compared to wild-type. **(A)** Initial activity without DTT additions in the assay, **(B)** maximal activity with 10 mM DTT included in the assay, **(C)** redox-activation state (initial/maximal activity*100). Leaves were sampled at the end of night and end of day. Results are means ± SE, *n* = 24 (wild-type) or 12 (mutants) independent plant replicates. Plants were grown in an 8 h photoperiod with 160 µmol photons m^{-2} s^{-1}. *: P<0.05, **: P<0.01, ***: P<0.001 (according to Student´s *t*-test)

Figure 9: Changes in the accumulation of starch and sucrose and in the thiol-disulfide reduction state of the small subunits of ADP-glucose pyrophosphorylase (APS1) in leaves of *trxf1*, *ntrc* and *trxf1 ntrc* Arabidopsis mutants compared to wild-type. **(A)** Starch level, **(B)** sucrose level, **(C)** starch/sucrose ratio, and **(D)** APS1 monomerisation (APS1 monomer as percent of total APS1 [monomer + dimer]) were measured in leaves sampled at the end of night (EN) and end of day (ED). APS1 monomerisation was analyzed in non-reducing SDS gels, where reduced and oxidized APS1 can be separated as monomer and dimer, respectively. Results are means ± SE, *n* = 8 (wild-type) or 4 (mutants) independent plant replicates growing in an 8 h photoperiod with 160 µmol photons m^{-2} s^{-1}. *: P<0.05, **: P<0.01, ***: P<0.001 (according to Student's *t*-test)

Figure 10: Changes in the in-vivo levels of phosphorylated intermediates in leaves of *trxf1*, *ntrc* and *trxf1 ntrc* Arabidopsis mutants compared to wild-type. **(A)** 3-phosphoglycerate (3PGA) level, **(B)** fructose 1,6-bisphosphate (FBP) level, **(C)** fructose 6-phosphate (F6P) level, **(D)** F6P/FBP ratio, **(E)** glucose 6-phosphate (G6P) level, and **(F)** glucose 1-phosphate (G1P) level were measured in leaves sampled at the end of the night and end of the day. Results are means ± SE, *n* = 20-30 (wild-type) or 10-15 (mutants) independent plant replicates growing in an 8 h photoperiod with 160 µmol photons m^{-2} s^{-1}. *: P<0.05, **: P<0.01, ***: P<0.001 (according to Student's *t*-test); n.d. = not detectable (values were below the detection limit)

Figure 11: Overview of changes in metabolite profiles from leaves of *trxf1*, *ntrc* and *trxf1 ntrc* Arabidopsis mutants compared to wild-type. Results from leaves sampled at the end of day **(A)** and end of night **(B)** are visualized using Vanted diagrams. Metabolite levels which are significantly different from wild-type according to the Student's *t*-test (P<0.05) are indicated in blue (increase) or red (decrease) color, while black color indicates no significant difference from wild-type. The order of the squares from left to right is *trxf1*, *ntrc* and *trxf1 ntrc* mutants being in first, second and third position, respectively. Data are taken from Supplemental Tables S4 – S7.

Figure 12: Suborganellar co-localization of Trx *f*1 and NTRC proteins. Co-localization of Trx*f*1:YFP and NTRC:CFP fusions in transiently transformed leaf mesophyll cells of *Nicotiana benthamiana*. The red auto-fluorescence of chlorophyll,

yellow fluorescence of YFP, blue fluorescence of CFP and the merge of the three fluorescent images are shown from left to right. Pictures were monitored in the channel mode with identical microscope settings. Bars = 10 µm

SUPPLEMENTAL FIGURES

Suppl. Figure S1: Changes in chlorophyll content in leaves of *trxf1*, *ntrc* and *trxf1 ntrc* Arabidopsis mutants compared to wild-type. Results are the mean ± SE, *n* = 10 (wild-type) or 5 (mutants) different plant replicates growing in an 8 h photoperiod with 160 µmol photons m^{-2} s^{-1}. *: P<0.05, **: P<0.01, ***: P<0.001 (according to Student's *t*-test)

Suppl. Figure S2: Histochemical localization of GUS expression in Arabidopsis plants transformed with a Trx*f*1$_{pro}$-GUS reporter gene. GUS staining of 10-day-old seedlings grown in a 16 h photoperiod **(A)** to **(D),** and of 6-week-old plants having flowered and begun to set seed **(E)** to **(I)**. GUS staining is shown in emerging leaves **(A)** and **(B)**, roots **(C)**, hypocotyl **(D)**, silique petiol **(E)**, silique **(F)**, flower **(G)**, sepal **(H)** and stigma **(I)**. No GUS staining was observed in trichomes **(B)**. The following microscopic techniques were used: **(A)**, **(E)** and **(F)** Stereomicroscopy, **(B)**, **(C)**, **(D)**, **(G)**, **(H)** and **(I)** differential interference contrast microscopy, and **(G)** and **(H)** single image merge. Bars = 1000 µm in **(A)**, **(E)**, **(F)**, **(G)** and **(H)**, and 100 µm in **(B)**, **(C)**, **(D)** and **(I)**.

SUPPLEMENTAL TABLES

Suppl. Table S1: Statistical analysis for rosette fresh weights of *trxf1*, *ntrc* and *trxf1 ntrc* Arabidopsis mutants growing in different light conditions, compared to wild-type. Values are based on the data presented in Figure 2H. Significantly different values from wild-type according to the Student's *t*-test are indicated in bold (P<0.05). n.d. = not detectable.

Suppl. Table S2: Statistical analysis for gas exchange parameters of *trxf1*, *ntrc* and *trxf1 ntrc* Arabidopsis mutants dependent on different light intensities, compared to wild-type. Values are based on the data presented in Figure 3. Significantly different

values from wild-type according to the Student´s *t*-test (P<0.05) are indicated in bold. PAR = photosynthetic active radiation.

Suppl. Table S3: Statistical analysis for the time course of fructose-1-6-bisphosphatase light activation in leaves of *trxf1*, *ntrc* and *trxf1 ntrc* Arabidopsis mutants, compared to wild-type. Values are based on the data presented in Figure 7D-F. Significantly different values from wild-type according to the Student´s *t*-test (P<0.05) are indicated in bold.

Suppl. Table S4: Changes in GC-MS based metabolite profiles in leaves of *trxf1*, *ntrc* and *trxf1 ntrc* Arabidopsis mutants compared to wild-type. Leaves were sampled at the end of the day. Results are means ± SD, *n* = 12. Values which are significantly different from wild-type according to the Student´s *t*-test (P<0.05) are indicated in bold (see also Figure 11A).

Suppl. Table S5: Changes in GC-MS based metabolite profiles in leaves of *trxf1*, *ntrc* and *trxf1 ntrc* Arabidopsis mutants compared to wild-type. Leaves were sampled at the end of the night. Results are means ± SD, *n* = 12. Values which are significantly different from wild-type according to the Student´s *t*-test (P<0.05) are indicated in bold (see also Figure 11B).

Suppl. Table S6: Changes in the levels of phosphorylated intermediates and starch in leaves of *trxf1*, *ntrc* and *trxf1 ntrc* Arabidopsis mutants compared to wild-type, based on spectrophotometric measurements. Leaves were sampled at the end of the day. Results are normalized to wild-type level and represent means ± SE, *n* = 8-30 (wild-type) or 4-15 (mutants). Values which are significantly different from wild-type according to the Student´s *t*-test (*P*<0.05) are indicated in bold (see Figure 11A).

Suppl. Table S7: Changes in the levels of phosphorylated intermediates and starch in leaves of *trxf1*, *ntrc* and *trxf1 ntrc* Arabidopsis mutants compared to wild-type, based on spectrophotometric measurements. Leaves were sampled at the end of the night. Results are normalized to wild-type level and represent means ± SE, *n* = 8-30 (wild-type) or 4-15 (mutants). Values which are significantly different from wild-type

according to the Student´s t-test ($P<0.05$) are indicated in bold (see also Figure 11B).

n.d. = not detectable.

Parsed Citations

Arsova, B., Hoja, U., Wimmelbacher, M., Greiner, E., Ustun, S., Melzer, M., Petersen, K., Lein, W., and Boernke, F. (2010). Plastidial thioredoxin z interacts with two fructokinase-like proteins in a thiol-dependent manner: Evidence for an essential role in chloroplast development in Arabidopsis and Nicotiana benthamiana. Plant Cell 22, 1498-1515.

Pubmed: Author and Title
CrossRef: Author and Title
Google Scholar: Author Only Title Only Author and Title

Ballicora, M.A., Frueauf, J.B., Fu, Y., Schürmann, P., and Preiss, J. (2000). Activation of the potato tuber ADP-glucose pyrophosphorylase by thioredoxin. J Biol Chem 275, 1315-1320.

Pubmed: Author and Title
CrossRef: Author and Title
Google Scholar: Author Only Title Only Author and Title

Balmer, Y., Koller, A, del Val, G., Manieri, W., Schürmann, P., and Buchanan, B.B. (2003). Proteomics gives insight into the regulatory function of chloroplast thioredoxins. Proc Natl Acad Sci USA 100, 370-375.

Pubmed: Author and Title
CrossRef: Author and Title
Google Scholar: Author Only Title Only Author and Title

Baumann, U., and Juttner, J. (2002). Plant thioredoxins: the multiplicity conundrum. Cell Mol Life Sci 59, 1042-1057.

Pubmed: Author and Title
CrossRef: Author and Title
Google Scholar: Author Only Title Only Author and Title

Beeler, S., Liu, H.-C., Stadler, M., Schreier, T., Eicke, S., Lue, W.-L., Truernit, E., Zeeman, S.C., Chen, J., and Kötting, O. (2014). Plastidial NAD-dependent malate dehydrogenase is critical for embryo development and heterotrophic metabolism in Arabidopsis. Plant Physiol 164, 1175-1190.

Pubmed: Author and Title
CrossRef: Author and Title
Google Scholar: Author Only Title Only Author and Title

Benitez-Alfonso, Y., Cilia, M., Roman, A.S., Thomas, C., Maule, A., Hearn, S., and Jackson, D. (2009). Control of Arabidopsis meristem development by thioredoxin-dependent regulation of intercellular transport. Proc Natl Acad Sci USA 106, 3615-3620.

Pubmed: Author and Title
CrossRef: Author and Title
Google Scholar: Author Only Title Only Author and Title

Bernal-Bayard, P., Ojeda, V., Hervas, M., Cejudo, F.J., Navarro, J.A., Velazquez-Campoy, A., and Perez-Ruiz, J.M. (2014). Molecular recognition in the interaction of chloroplast 2-Cys peroxiredoxin with NADPH-thioredoxin reductase C (NTRC) and thioredoxin x. FEBS Lett 588, 4342-4347.

Pubmed: Author and Title
CrossRef: Author and Title
Google Scholar: Author Only Title Only Author and Title

Bohrer, A.-S., Massot, V., Innocenti, G., Reichheld, J.-P., Issakidis-Bourguet, E., and Vanacker, H. (2012). New insights into the reduction systems of plastidial thioredoxins point out the unique properties of thioredoxin z from Arabidopsis. J Exp Bot 63, 6315-6323.

Pubmed: Author and Title
CrossRef: Author and Title
Google Scholar: Author Only Title Only Author and Title

Buchanan, B.B. (1980). Role of light in the regulation of chloroplast enzymes. Annu Rev Plant Physiol 31, 341-374.

Pubmed: Author and Title
CrossRef: Author and Title
Google Scholar: Author Only Title Only Author and Title

Buchanan, B.B., and Balmer, Y. (2005). Redox regulation: a broadening horizon. Annu Rev Plant Biol 56, 187-220.

Pubmed: Author and Title
CrossRef: Author and Title
Google Scholar: Author Only Title Only Author and Title

Buchanan, B.B., Wolosiuk, R.A, and Schürmann, P. (1979). Thioredoxin and enzyme regulation. Trends Biochem Sci 4, 93-96.

Pubmed: Author and Title
CrossRef: Author and Title
Google Scholar: Author Only Title Only Author and Title

Carrari F., Coll-Garcia D., Schauer N., Lytovchenko A., Palacios-Rojas N., Balbo I., Rosso M, and Fernie AR (2005). Deficiency of a plastidial adenylate kinase in Arabidopsis results in elevated photosynthetic amino acid biosynthesis and enhanced growth. Plant Physiol 137, 70-82.

Pubmed: Author and Title
CrossRef: Author and Title
Google Scholar: Author Only Title Only Author and Title

Chiadmi, M., Navaza, A., Miginiac-Maslow, M., Jacquot, J.P., and Cherfils, J. (1999). Redox signalling in the chloroplast: structure of oxidized pea fructose-1,6-bisphosphate phosphatase. EMBO J 18, 6809-6815.

Pubmed: Author and Title
CrossRef: Author and Title

Google Scholar: Author Only Title Only Author and Title

Chibani, K., Tarrago, L., Schuermann, P., Jacquot, J.-P., and Rouhier, N. (2011). Biochemical properties of poplar thioredoxin z. Febs Letters 585, 1077-1081.
Pubmed: Author and Title
CrossRef: Author and Title
Google Scholar: Author Only Title Only Author and Title

Choi, Y.A., Kim, S.G., and Kwon, Y.M. (1999). The plastidic glutamine synthetase activity is directly modulated by means of redox change at two unique cysteine residues. Plant Sci 149, 175-182.
Pubmed: Author and Title
CrossRef: Author and Title
Google Scholar: Author Only Title Only Author and Title

Clough, S.J., and Bent, A.F. (1998). Floral dip: a simplified method for Agrobacterium-mediated transformation of Arabidopsis thaliana. Plant J 16, 735-743.
Pubmed: Author and Title
CrossRef: Author and Title
Google Scholar: Author Only Title Only Author and Title

Collin, V., Issakidis-Bourguet, E., Marchand, C., Hirasawa, M., Lancelin, J.M., Knaff, D.B., and Miginiac-Maslow, M. (2003). The Arabidopsis plastidial thioredoxins - New functions and new insights into specificity. J Biol Chem 278, 23747-23752.
Pubmed: Author and Title
CrossRef: Author and Title
Google Scholar: Author Only Title Only Author and Title

Collin, V., Lamkemeyer, P., Miginiac-Maslow, M., Hirasawa, M., Knaff, D.B., Dietz, K.-J., and Issakidis-Bourguet, E. (2004). Characterization of plastidial thioredoxins from Arabidopsis belonging to the new y-type. Plant Physiol 136, 4088-4095.
Pubmed: Author and Title
CrossRef: Author and Title
Google Scholar: Author Only Title Only Author and Title

Cook, K.M., and Hogg, P.J. (2013). Post-translational control of protein function by disulfide bond cleavage. Antioxid Redox Signal 18, 1987-2015.
Pubmed: Author and Title
CrossRef: Author and Title
Google Scholar: Author Only Title Only Author and Title

Courteille, A., Vesa, S., Sanz-Barrio, R., Cazale, A.-C., Becuwe-Linka, N., Farran, I., Havaux, M., Rey, P., and Rumeau, D. (2013). Thioredoxin m4 controls photosynthetic alternative electron pathways in Arabidopsis. Plant Physiol 161, 508-520.
Pubmed: Author and Title
CrossRef: Author and Title
Google Scholar: Author Only Title Only Author and Title

Dietz, K.-J., and Pfannschmidt, T. (2011). Novel regulators in photosynthetic redox control of plant metabolism and gene expression. Plant Physiol 155, 1477-1485.
Pubmed: Author and Title
CrossRef: Author and Title
Google Scholar: Author Only Title Only Author and Title

Faix, B., Radchuk, V., Nerlich, A., Hummer, C., Radchuk, R., Emery, R.J., Keller, H., Gotz, K.P., Weschke, W., Geigenberger, P., and Weber, H. (2012). Barley grains, deficient in cytosolic small subunit of ADP-glucose pyrophosphorylase, reveal coordinate adjustment of C:N metabolism mediated by an overlapping metabolic-hormonal control. Plant J 69, 1077-1093.
Pubmed: Author and Title
CrossRef: Author and Title
Google Scholar: Author Only Title Only Author and Title

Faske, M., Holtgrefe, S., Ocheretina, O., Meister, M., Backhausen, J.E., and Scheibe, R. (1995). Redox equilibria between the regulatory thiols of light/dark-modulated chloroplast enzymes and dithiothreitol: fine-tuning by metabolites. Biochim Biophys Acta 1247, 135-142.
Pubmed: Author and Title
CrossRef: Author and Title
Google Scholar: Author Only Title Only Author and Title

Fernie, A.R., Tiessen, A., Stitt, M., Willmitzer, L., and Geigenberger, P. (2002). Altered metabolic fluxes result from shifts in metabolite levels in sucrose phosphorylase-expressing potato tubers. Plant Cell Environ 25, 1219-1232.
Pubmed: Author and Title
CrossRef: Author and Title
Google Scholar: Author Only Title Only Author and Title

Fu, Y., Ballicora, M.A., Leykam, J.F., and Preiss, J. (1998). Mechanism of Reductive activation of potato tuber ADP-glucose pyrophosphorylase. J Biol Chem 273, 25045-25052.
Pubmed: Author and Title
CrossRef: Author and Title
Google Scholar: Author Only Title Only Author and Title

Geigenberger, P., and Fernie, AR (2014). Metabolic control of redox and redox-control of metabolism in plants. Antioxid Redox Signal 21, 1389-1421.
Pubmed: Author and Title
CrossRef: Author and Title

Google Scholar: Author Only Title Only Author and Title

Geigenberger, P., Kolbe, A., and Tiessen, A. (2005). Redox regulation of carbon storage and partitioning in response to light and sugars. J Exp Bot 56, 1469-1479.
Pubmed: Author and Title
CrossRef: Author and Title
Google Scholar: Author Only Title Only Author and Title

Glaring, M.A., Skryhan, K., Kotting, O., Zeeman, S.C., and Blennow, A. (2012). Comprehensive survey of redox sensitive starch metabolising enzymes in Arabidopsis thaliana. Plant Physiol Biochem 58, 89-97.
Pubmed: Author and Title
CrossRef: Author and Title
Google Scholar: Author Only Title Only Author and Title

Grieco, M., Tikkanen, M., Paakkarinen, V., Kangasjarvi, S., and Aro, E.M. (2012). Steady-state phosphorylation of light-harvesting complex II proteins preserves photosystem I under fluctuating white light. Plant Physiol 160, 1896-1910.
Pubmed: Author and Title
CrossRef: Author and Title
Google Scholar: Author Only Title Only Author and Title

Hädrich N, Hendriks JHM, Kötting O, Arrivault S, Feil R, Zeeman SC, Gibon Y, Schulze WX, Stitt M, Lunn JE (2012). Mutagenesis of cysteine 81 prevents dimerization of the APS1 subunit of ADP-glucose pyrophosphorylase and alters diurnal starch turnover in Arabidopsis thaliana leaves. Plant J 70, 231-242.
Pubmed: Author and Title
CrossRef: Author and Title
Google Scholar: Author Only Title Only Author and Title

Hendriks, J.H.M., Kolbe, A., Gibon, Y., Stitt, M., and Geigenberger, P. (2003). ADP-glucose pyrophosphorylase is activated by posttranslational redox-modification in response to light and to sugars in leaves of Arabidopsis and other plant species. Plant Physiol 133, 838-849.
Pubmed: Author and Title
CrossRef: Author and Title
Google Scholar: Author Only Title Only Author and Title

Hertle, A.P., Blunder, T., Wunder, T., Pesaresi, P., Pribil, M., Armbruster, U., and Leister, D. (2013). PGRL1 is the elusive ferredoxin-plastoquinone reductase in photosynthetic cyclic electron flow. Mol Cell 49, 511-523.
Pubmed: Author and Title
CrossRef: Author and Title
Google Scholar: Author Only Title Only Author and Title

Hodges, M., Miginiac-Maslow, M., Decottignies, P., Jacquot, J.-P., Stein, M., Lepiniec, L., Crétin, C., and Gadal, P. (1994). Purification and characterization of pea thioredoxin f expressed in Escherichia coli. Plant Mol Biol 26, 225-234.
Pubmed: Author and Title
CrossRef: Author and Title
Google Scholar: Author Only Title Only Author and Title

Holaday, A.S., Martindale, W., Alred, R., Brooks, A.L., and Leegood, R.C. (1992). Changes in activities of enzymes of carbon metabolism in leaves during exposure of plants to low temperature. Plant Physiol 98, 1105-1114.
Pubmed: Author and Title
CrossRef: Author and Title
Google Scholar: Author Only Title Only Author and Title

Holmgren, A. (1985). Thioredoxin. Annu Rev Biochem 54, 237-271.
Pubmed: Author and Title
CrossRef: Author and Title
Google Scholar: Author Only Title Only Author and Title

Ikegami, A., Yoshimura, N., Motohashi, K., Takahashi, S., Romano, P.G.N., Hisabori, T., Takamiya, K.-I., and Masuda, T. (2007). The CHLI1 subunit of Arabidopsis thaliana magnesium chelatase is a target protein of the chloroplast thioredoxin. J Biol Chem 282, 19282-19291.
Pubmed: Author and Title
CrossRef: Author and Title
Google Scholar: Author Only Title Only Author and Title

Jefferson, R.A., Kavanagh, T.A., and Bevan, M.W. (1987). GUS fusions: beta-glucuronidase as a sensitive and versatile gene fusion marker in higher plants. EMBO J 6, 3901-3907.
Pubmed: Author and Title
CrossRef: Author and Title
Google Scholar: Author Only Title Only Author and Title

Jelitto, T., Sonnewald, U., Willmitzer, L., Hajirezeai, M., and Stitt, M. (1992). Inorganic pyrophosphate content and metabolites in potato and tobacco plants expressing E. coli pyrophosphatase in their cytosol. Planta 188, 238-244.
Pubmed: Author and Title
CrossRef: Author and Title
Google Scholar: Author Only Title Only Author and Title

Kirchsteiger, K., Ferrandez, J., Pascual, M.B., Gonzalez, M., and Cejudo, F.J. (2012). NADPH thioredoxin reductase C is localized in plastids of photosynthetic and nonphotosynthetic tissues and is involved in lateral root formation in Arabidopsis. Plant Cell 24, 1534-1548.
Pubmed: Author and Title

CrossRef: Author and Title
Google Scholar: Author Only Title Only Author and Title

Kolbe, A., Tiessen, A., Schluepmann, H., Paul, M., Ulrich, S., and Geigenberger, P. (2005). Trehalose 6-phosphate regulates starch synthesis via posttranslational redox activation of ADP-glucose pyrophosphorylase. Proc Natl Acad Sci USA 102, 11118-11123.
Pubmed: Author and Title
CrossRef: Author and Title
Google Scholar: Author Only Title Only Author and Title

Koßmann, J., Sonnewald, U., and Willmitzer, L. (1994). Reduction of the chloroplastic fructose-1,6-bisphosphatase in transgenic potato plants impairs photosynthesis and plant growth.Plant J 6, 637-650.
Pubmed: Author and Title
CrossRef: Author and Title
Google Scholar: Author Only Title Only Author and Title

Laemmli, U.K. (1970). Cleavage of structural proteins during the assembly of the head of bacteriophage T4. Nature 227, 680-685.
Pubmed: Author and Title
CrossRef: Author and Title
Google Scholar: Author Only Title Only Author and Title

Lepisto, A., Pakula, E., Toivola, J., Krieger-Liszkay, A., Vignols, F., and Rintamaki, E. (2013). Deletion of chloroplast NADPH-dependent thioredoxin reductase results in inability to regulate starch synthesis and causes stunted growth under short-day photoperiods. J Exp Bot 64, 3843-3854.
Pubmed: Author and Title
CrossRef: Author and Title
Google Scholar: Author Only Title Only Author and Title

Lepisto, A., Kangasjarvi, S., Luomala, E.-M., Brader, G., Sipari, N., Keranen, M., Keinanen, M., and Rintamaki, E. (2009). Chloroplast NADPH-thioredoxin reductase interacts with photoperiodic development in Arabidopsis. Plant Physiol 149, 1261-1276.
Pubmed: Author and Title
CrossRef: Author and Title
Google Scholar: Author Only Title Only Author and Title

Lichter, A., and Häberlein, I. (1998). A light-dependent redox signal participates in the regulation of ammonia fixation in chloroplasts of higher plants — ferredoxin: Glutamate synthase is a thioredoxin-dependent enzyme. J Plant Physiol 153, 83-90.
Pubmed: Author and Title
CrossRef: Author and Title
Google Scholar: Author Only Title Only Author and Title

Lintala, M., Schuck, N., Thormählen, I., Jungfer, A., Weber, K.L., Weber, A.P., Geigenberger, P., Soll, J., Bolter, B., and Mulo, P. (2014). Arabidopsis tic62 trol mutant lacking thylakoid-bound ferredoxin-NADP+ oxidoreductase shows distinct metabolic phenotype. Mol Plant 7, 45-57.
Pubmed: Author and Title
CrossRef: Author and Title
Google Scholar: Author Only Title Only Author and Title

Liu, Y.J., Norberg, F.E., Szilagyi, A., De Paepe, R., Akerlund, H.E., and Rasmusson, A.G. (2008). The mitochondrial external NADPH dehydrogenase modulates the leaf NADPH/NADP+ ratio in transgenic Nicotiana sylvestris. Plant Cell Physiol 49, 251-263.
Pubmed: Author and Title
CrossRef: Author and Title
Google Scholar: Author Only Title Only Author and Title

Livingston, A.K., Cruz, J.A., Kohzuma, K., Dhingra, A., and Kramer, D.M. (2010). An Arabidopsis mutant with high cyclic electron flow around photosystem I (hcef) involving the NADPH dehydrogenase complex. Plant Cell 22, 221-233.
Pubmed: Author and Title
CrossRef: Author and Title
Google Scholar: Author Only Title Only Author and Title

Luo, T., Fan, T., Liu, Y., Rothbart, M., Yu, J., Zhou, S., Grimm, B., and Luo, M. (2012). Thioredoxin redox-regulates ATPase activity of magnesium chelatase CHLI subunit and modulates redox-mediated signaling in tetrapyrrol biosynthesis and homeostasis of reactive oxygen species in pea plants. Plant Physiol 159, 118-130.
Pubmed: Author and Title
CrossRef: Author and Title
Google Scholar: Author Only Title Only Author and Title

Meyer, Y., Belin, C., Delorme-Hinoux, V., Reichheld, J.-P., and Riondet, C. (2012). Thioredoxin and glutaredoxin systems in plants: molecular mechanisms, crosstalks, and functional significance. Antioxid Redox Signal 17, 1124-1160.
Pubmed: Author and Title
CrossRef: Author and Title
Google Scholar: Author Only Title Only Author and Title

Michalska, J., Zauber, H., Buchanan, B.B., Cejudo, F.J., and Geigenberger, P. (2009). NTRC links built-in thioredoxin to light and sucrose in regulating starch synthesis in chloroplasts and amyloplasts. Proc Natl Acad Sci USA 106, 9908-9913.
Pubmed: Author and Title
CrossRef: Author and Title
Google Scholar: Author Only Title Only Author and Title

Michelet, L., Zaffagnini, M., Morisse, S., Sparla, F., Perez-Perez, M.E., Francia, F., Danon, A., Marchand, C.H., Fermani, S., Trost, P., and Lemaire, S.D. (2013). Redox regulation of the Calvin-Benson cycle: something old, something new. Front Plant Sci 4, 470.
Pubmed: Author and Title

CrossRef: Author and Title
Google Scholar: Author Only Title Only Author and Title

Mikkelsen, R., Mutenda, K.E., Mant, A., Schurmann, P., and Blennow, A. (2005). Alpha-glucan, water dikinase (GWD): a plastidic enzyme with redox-regulated and coordinated catalytic activity and binding affinity. Proc Natl Acad Sci USA 102, 1785-1790.
Pubmed: Author and Title
CrossRef: Author and Title
Google Scholar: Author Only Title Only Author and Title

Mugford, S.T., Fernandez, O., Brinton, J., Flis, A., Krohn, N., Encke, B., Feil, R., Sulpice, R., Lunn, JE, Stitt, M., and Smith A.M. (2014). Regulatory properties of ADP glucose pyrophosphorylase are required for adjustment of leaf starch synthesis in different photoperiods. Plant Physiol 166, 1733-1747.
Pubmed: Author and Title
CrossRef: Author and Title
Google Scholar: Author Only Title Only Author and Title

Nee, G., Zaffagnini, M., Trost, P., and Issakidis-Bourguet, E. (2009). Redox regulation of chloroplast glucose-6-phosphate dehydrogenase: a new role for f-type thioredoxin. FEBS Lett 583, 2827-2832
Pubmed: Author and Title
CrossRef: Author and Title
Google Scholar: Author Only Title Only Author and Title

Nikkanen, L., and Rintamäki, E. (2014). Thioredoxin-dependent regulatory networks in chloroplasts under fluctuating light conditions. Philosophical Transactions of the Royal Society B: Biological Sciences 369.
Pubmed: Author and Title
CrossRef: Author and Title
Google Scholar: Author Only Title Only Author and Title

Obana Y, Omoto D, Kato C, Matsumoto K, Nagai Y, Kavakli IH, Hamada S, Edwards GE, Okita TW, Matsui H, Ito H (2006). Enhanced turnover of transitory starch by expression of up-regulated ADP-glucose pyrophosphorylases in Arabidopsis thaliana. Plant Sci 170, 1-11.
Pubmed: Author and Title
CrossRef: Author and Title
Google Scholar: Author Only Title Only Author and Title

Perez-Ruiz, J.M., Guinea, M., Puerto-Galan, L., and Cejudo, F.J. (2014). NADPH thioredoxin reductase C is involved in redox regulation of the Mg-chelatase I subunit in Arabidopsis thaliana chloroplasts. Mol Plant 7, 1252-1255.
Pubmed: Author and Title
CrossRef: Author and Title
Google Scholar: Author Only Title Only Author and Title

Perez-Ruiz, J.M., Gonzalez, M., Spinola, M.C., Sandalio, L.M., and Cejudo, F.J. (2009). The quaternary structure of NADPH thioredoxin reductase C is redox-sensitive. Mol Plant 2, 457-467.
Pubmed: Author and Title
CrossRef: Author and Title
Google Scholar: Author Only Title Only Author and Title

Perez-Ruiz, J.M., Spinola, M.C., Kirchsteiger, K., Moreno, J., Sahrawy, M., and Cejudo, F.J. (2006). Rice NTRC is a high-efficiency redox system for chloroplast protection against oxidative damage. Plant Cell 18, 2356-2368.
Pubmed: Author and Title
CrossRef: Author and Title
Google Scholar: Author Only Title Only Author and Title

Pérez-Ruiz, J.M., and Cejudo, F.J. (2009). A proposed reaction mechanism for rice NADPH thioredoxin reductase C, an enzyme with protein disulfide reductase activity. FEBS Lett 583, 1399-1402.
Pubmed: Author and Title
CrossRef: Author and Title
Google Scholar: Author Only Title Only Author and Title

Pfannschmidt, T., and Liere, K. (2005). Redox regulation and modification of proteins controlling chloroplast gene expression. Antioxid Redox Signal 7, 607-618.
Pubmed: Author and Title
CrossRef: Author and Title
Google Scholar: Author Only Title Only Author and Title

Porra, R.J., Thompson, W.A., and Kriedemann, P.E. (1989). Determination of accurate extinction coefficients and simultaneous equations for assaying chlorophylls a and b extracted with four different solvents: verification of the concentration of chlorophyll standards by atomic absorption spectroscopy. Biochim Biophys Acta 975, 384-394.
Pubmed: Author and Title
CrossRef: Author and Title
Google Scholar: Author Only Title Only Author and Title

Preiss, J. (1988) Biosynthesis of starch and its regulation. In J Preiss, ed, The Biochemistry of Plants, Vol 14. Academic Press, New York, pp 181-254
Pubmed: Author and Title
CrossRef: Author and Title
Google Scholar: Author Only Title Only Author and Title

Richter, A.S., Peter, E., Rothbart, M., Schlicke, H., Toivola, J., Rintamaki, E., and Grimm, B. (2013). Posttranslational influence of NADPH-dependent thioredoxin reductase C on enzymes in tetrapyrrole synthesis. Plant Physiol 162, 63-73.

Pubmed: Author and Title
CrossRef: Author and Title
Google Scholar: Author Only Title Only Author and Title

Rojas-Gonzalez, J.A., Soto-Suarez, M., Garcia-Diaz, A., Romero-Puertas, M.C., Sandalio, L.M., Merida, A., Thormählen, I., Geigenberger, P., Serrato, A. J., and Sahrawy, M. (2015). Disruption of both chloroplastic and cytosolic FBPase genes results in a dwarf phenotype and important starch and metabolite changes in Arabidopsis thaliana. J Exp Bot 66, 2673-2689.
Pubmed: Author and Title
CrossRef: Author and Title
Google Scholar: Author Only Title Only Author and Title

Sasaki, Y., Kozaki, A., and Hatano, M. (1997). Link between light and fatty acid synthesis: thioredoxin-linked reductive activation of plastidic acetyl-CoA carboxylase. Proc Natl Acad Sci USA 94, 11096-11101.
Pubmed: Author and Title
CrossRef: Author and Title
Google Scholar: Author Only Title Only Author and Title

Scheibe, R. (2004). Malate valves to balance cellular energy supply. Physiol Plant 120, 21-26.
Pubmed: Author and Title
CrossRef: Author and Title
Google Scholar: Author Only Title Only Author and Title

Scheibe, R., and Stitt, M. (1988). Comparison of NADP-malate dehydrogenase activation, QA reduction and O2 evolution in spinach leaves. Plant Physiol Biochem 26, 473-481.
Pubmed: Author and Title
CrossRef: Author and Title
Google Scholar: Author Only Title Only Author and Title

Schmitz, J., Heinrichs, L., Scossa, F., Fernie, A.R., Oelze, M.L., Dietz, K.J., Rothbart, M., Grimm, B., Flugge, U.I., and Hausler, R.E. (2014). The essential role of sugar metabolism in the acclimation response of Arabidopsis thaliana to high light intensities. J Exp Bot 65, 1619-1636.
Pubmed: Author and Title
CrossRef: Author and Title
Google Scholar: Author Only Title Only Author and Title

Schuermann, P., and Buchanan, B.B. (2008). The ferredoxin/thioredoxin system of oxygenic photosynthesis. Antioxid Redox Signal 10, 1235-1273.
Pubmed: Author and Title
CrossRef: Author and Title
Google Scholar: Author Only Title Only Author and Title

Schwarz, C., Bohne, A.-V., Wang, F., Javier Cejudo, F., and Nickelsen, J. (2012). An intermolecular disulfide-based light switch for chloroplast psbD gene expression in Chlamydomonas reinhardtii. Plant J 72, 378-389.
Pubmed: Author and Title
CrossRef: Author and Title
Google Scholar: Author Only Title Only Author and Title

Serrato, A.J., Perez-Ruiz, J.M., Spinola, M.C., and Cejudo, F.J. (2004). A novel NADPH thioredoxin reductase, localized in the chloroplast, which deficiency causes hypersensitivity to abiotic stress in Arabidopsis thaliana. J Biol Chem 279, 43821-43827.
Pubmed: Author and Title
CrossRef: Author and Title
Google Scholar: Author Only Title Only Author and Title

Seung, D., Thalmann, M., Sparla, F., Abou Hachem, M., Lee, S.K., Issakidis-Bourguet, E., Svensson, B., Zeeman, S.C., and Santelia, D. (2013). Arabidopsis thaliana AMY3 is a unique redox-regulated chloroplastic alpha-amylase. J Biol Chem 288, 33620-33633.
Pubmed: Author and Title
CrossRef: Author and Title
Google Scholar: Author Only Title Only Author and Title

Silver, D.M., Silva, L.P., Issakidis-Bourguet, E., Glaring, M.A., Schriemer, D.C., and Moorhead, G.B. (2013). Insight into the redox regulation of the phosphoglucan phosphatase SEX4 involved in starch degradation. FEBS J 280, 538-548.
Pubmed: Author and Title
CrossRef: Author and Title
Google Scholar: Author Only Title Only Author and Title

Stitt, M., Lilley, R.M., Gerhardt, R., and Heldt, H.W. (1989). Metabolite levels in specific cells and subcellular compartments of plant leaves. In Methods in Enzymology, B.F. Sidney Fleischer, ed (Academic Press), pp. 518-552.
Pubmed: Author and Title
CrossRef: Author and Title
Google Scholar: Author Only Title Only Author and Title

Suorsa, M., Jarvi, S., Grieco, M., Nurmi, M., Pietrzykowska, M., Rantala, M., Kangasjarvi, S., Paakkarinen, V., Tikkanen, M., Jansson, S., and Aro, E.M. (2012). PROTON GRADIENT REGULATION5 is essential for proper acclimation of Arabidopsis photosystem I to naturally and artificially fluctuating light conditions. Plant Cell 24, 2934-2948.
Pubmed: Author and Title
CrossRef: Author and Title
Google Scholar: Author Only Title Only Author and Title

Thormählen, I., Ruber, J., Von Roepenack-Lahaye, E., Ehrlich, S.M., Massot, V., Hummer, C., Tezycka, J., Issakidis-Bourguet, E., and Geigenberger, P. (2013). Inactivation of thioredoxin f1 leads to decreased light activation of ADP-glucose pyrophosphorylase

and altered diurnal starch turnover in leaves of Arabidopsis plants. Plant Cell Environ 36, 16-29.
Pubmed: Author and Title
CrossRef: Author and Title
Google Scholar: Author Only Title Only Author and Title

Tikkanen, M., and Aro, E.M. (2014). Integrative regulatory network of plant thylakoid energy transduction. Trends Plant Sci 19, 10-17.
Pubmed: Author and Title
CrossRef: Author and Title
Google Scholar: Author Only Title Only Author and Title

Tikkanen, M., Mekala, N.R., and Aro, E.M. (2014). Photosystem II photoinhibition-repair cycle protects Photosystem I from irreversible damage. Biochim Biophys Acta 1837, 210-215.
Pubmed: Author and Title
CrossRef: Author and Title
Google Scholar: Author Only Title Only Author and Title

Valerio, C., Costa, A., Marri, L., Issakidis-Bourguet, E., Pupillo, P., Trost, P., and Sparla, F. (2011). Thioredoxin-regulated beta-amylase (BAM1) triggers diurnal starch degradation in guard cells, and in mesophyll cells under osmotic stress. J Exp Bot 62, 545-555.
Pubmed: Author and Title
CrossRef: Author and Title
Google Scholar: Author Only Title Only Author and Title

Wang, P., Liu, J., Liu, B., Feng, D., Da, Q., Wang, P., Shu, S., Su, J., Zhang, Y., Wang, J., and Wang, H.B. (2013). Evidence for a role of chloroplastic m-type thioredoxins in the biogenesis of photosystem II in Arabidopsis. Plant Physiol 163, 1710-1728.
Pubmed: Author and Title
CrossRef: Author and Title
Google Scholar: Author Only Title Only Author and Title

Wulff, R.P., Lundqvist, J., Rutsdottir, G., Hansson, A., Stenbaek, A., Elmlund, D., Elmlund, H., Jensen, P.E., and Hansson, M. (2011). The activity of barley NADPH-dependent thioredoxin reductase C is independent of the oligomeric state of the protein: tetrameric structure determined by cryo-electron microscopy. Biochemistry 50, 3713-3723.
Pubmed: Author and Title
CrossRef: Author and Title
Google Scholar: Author Only Title Only Author and Title

Zakharov, A., Giersberg, M., Hosein, F., Melzer, M., Muntz, K., and Saalbach, I. (2004). Seed-specific promoters direct gene expression in non-seed tissue. J Exp Bot 55, 1463-1471.
Pubmed: Author and Title
CrossRef: Author and Title
Google Scholar: Author Only Title Only Author and Title

Zimmermann, G., Kelly, G.J., and Latzko, E. (1976). Efficient purification and molecular properties of spinach chloroplast fructose 1,6-bisphosphatase. Eur J Biochem 70, 361-367.
Pubmed: Author and Title
CrossRef: Author and Title
Google Scholar: Author Only Title Only Author and Title

Yoshida, K., Hara, S., and Hisabori, T. (2015). Thioredoxin selectivity for thiol-based redox regulation of target proteins in chloroplasts. J Biol Chem 290, 14278-14288.
Pubmed: Author and Title
CrossRef: Author and Title
Google Scholar: Author Only Title Only Author and Title

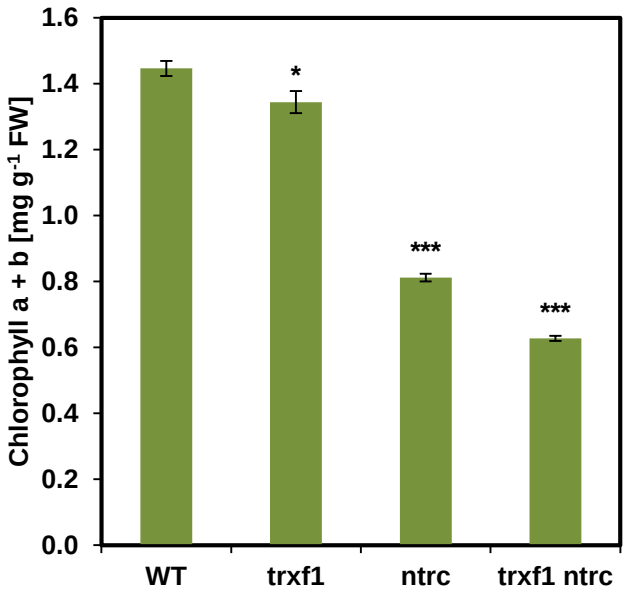

Suppl. Figure S1: Changes in chlorophyll content in leaves of *trxf1*, *ntrc* and *trxf1 ntrc* Arabidopsis mutants compared to wild-type. Results are the mean ± SE, *n* = 10 (wild-type) or 5 (mutants) different plant replicates growing in an 8 h photoperiod with 160 µmol photons m^{-2} s^{-1}. *: P<0.05, **: P<0.01, ***: P<0.001 (according to Student's *t*-test)

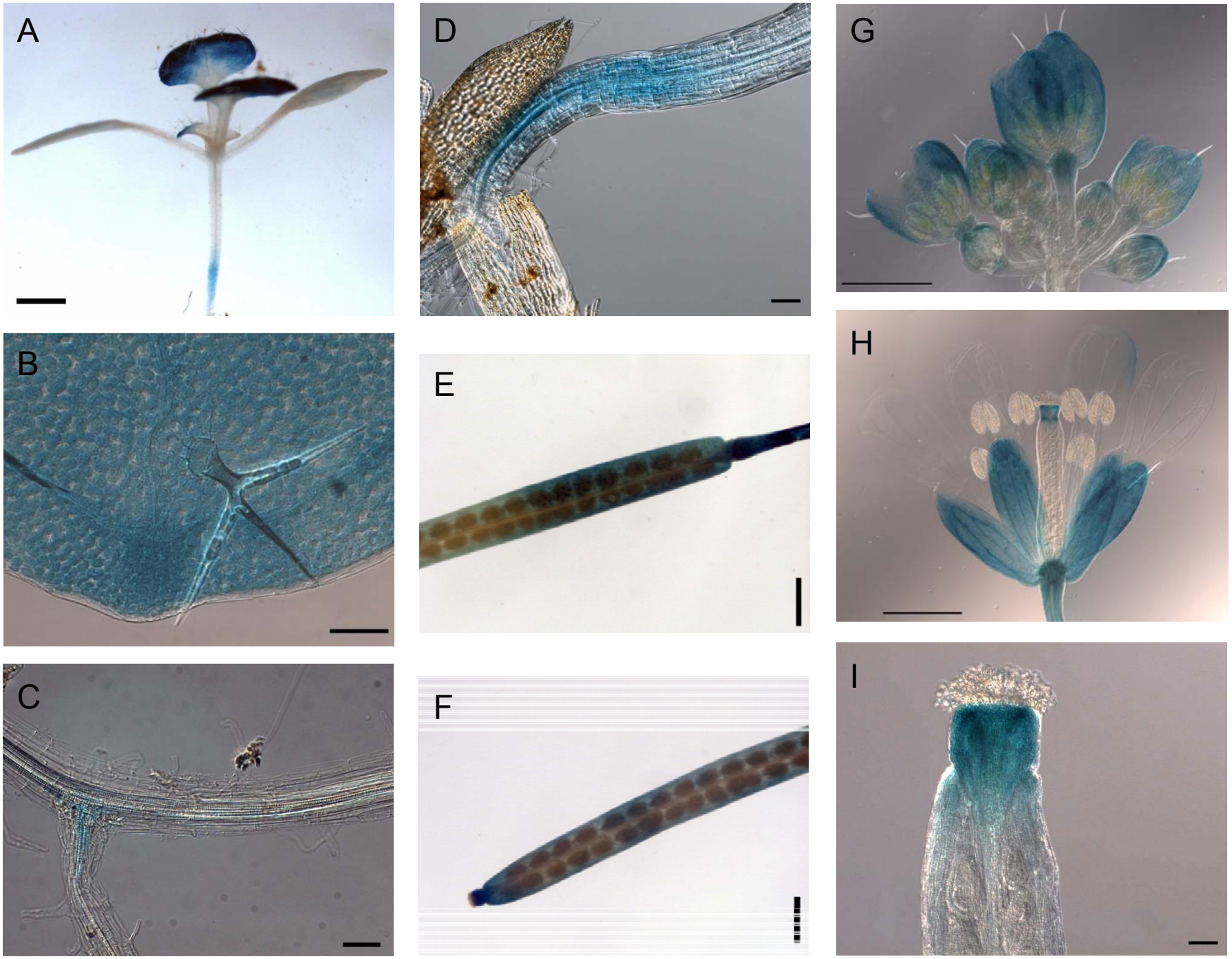
A
B
C
D
E
F
G
H
I

Suppl. Figure S2: Histochemical localization of GUS expression in Arabidopsis plants transformed with a Trx*f*1$_{pro}$-GUS reporter gene. GUS staining of 10-day-old seedlings grown in a 16 h photoperiod **(A)** to **(D),** and of 6-week-old plants having flowered and begun to set seed **(E)** to **(I)**. GUS staining is shown in emerging leaves **(A)** and **(B)**, roots **(C)**, hypocotyl **(D)**, silique petiol **(E)**, silique **(F)**, flower **(G)**, sepal **(H)** and stigma **(I)**. No GUS staining was observed in trichomes **(B)**. The following microscopic techniques were used: **(A)**, **(E)** and **(F)** Stereomicroscopy, **(B)**, **(C)**, **(D)**, **(G)**, **(H)** and **(I)** differential interference contrast microscopy, and **(G)** and **(H)** single image merge. Bars = 1000 µm in **(A)**, **(E)**, **(F)**, **(G)** and **(H)**, and 100 µm in **(B)**, **(C)**, **(D)** and **(I)**.

Suppl. Table S1:

Statistical analysis for rosette fresh weights of *trxf1*, *ntrc* and *trxf1 ntrc Arabidopsis* mutants growing in different light conditions, compared to wild-type. Values are based on the data presented in Figure 2H. Significantly different values from wild-type according to the Student's *t*-test ($P<0.05$) are indicated in bold. n.d. = not detectable. Growth conditions see Figure 2H.

Growth condition	*trxf1*	*ntrc*	*trxf1 ntrc*
4h-day, moderate light	**0.002**	**<0.001**	n.d.
8h-day, moderate light	0.354	**<0.001**	**<0.001**
16h-day, moderate light	0.484	**<0.001**	**<0.001**
24h-day, moderate light	0.316	**<0.001**	**<0.001**
8h-day, low light	**<0.001**	**<0.001**	n.d.
8h-day, high light	0.781	**<0.001**	**<0.001**

Suppl. Table S2:

Statistical analysis for gas exchange parameters of *trxf1*, *ntrc* and *trxf1 ntrc* Arabidopsis mutants dependent on different light intensities, compared to wild-type. Values are based on the data presented in Figure 3. Significantly different values from wild-type according to the Student's *t*-test ($P<0.05$) are indicated in bold. PAR = photosynthetically active radiation.

PAR [µmol m^{-2} s^{-1}]	Assimilation rate			Transpiration rate			Intercellular CO_2 mole fraction		
	trxf1	*ntrc*	*trxf1 ntrc*	*trxf1*	*ntrc*	*trxf1 ntrc*	*trxf1*	*ntrc*	*trxf1 ntrc*
0	0.402	0.365	**0.011**	0.767	0.773	**0.002**	0.328	0.912	0.693
50	0.958	**0.009**	**0.017**	0.789	0.971	**0.016**	0.446	0.063	**<0.001**
100	0.863	0.052	**0.004**	0.864	0.944	**0.022**	0.682	**0.046**	**<0.001**
150	0.762	0.081	**0.005**	0.882	0.906	**0.026**	0.996	**0.040**	**<0.001**
200	0.797	**0.048**	**0.008**	0.851	0.525	**0.037**	0.670	0.078	**<0.001**
300	0.576	0.091	**<0.001**	0.935	0.773	0.052	0.660	**0.040**	**<0.001**
400	0.455	0.090	**<0.001**	0.916	0.909	**0.033**	0.585	**0.047**	**<0.001**
600	0.532	0.058	**<0.001**	0.852	0.884	**0.029**	0.404	**0.026**	**<0.001**
800	0.529	0.104	**0.002**	0.794	0.638	**0.017**	0.208	0.087	**<0.001**
1000	0.493	0.077	0.071	0.718	0.456	**0.028**	0.170	0.056	**<0.001**

Supplemental Table S3:

Statistical analysis for the time course of fructose-1,6-bisphosphatase light activation in leaves of *trxf1*, *ntrc* and *trxf1 ntrc* *Arabidopsis* mutants, compared to wild-type. Values are based on the data presented in Figure 7D-F. Significantly different values from wild-type according to the Student's *t*-test ($P<0.05$) are indicated in bold. Time = time after illumination

Time [min]	Initial activity			Maximal activity			Activation state		
	trxf1	*ntrc*	*trxf1 ntrc*	*trxf1*	*ntrc*	*trxf1 ntrc*	*trxf1*	*ntrc*	*trxf1 ntrc*
0	0.802	0.503	0.070	0.837	0.811	**0.014**	0.521	0.480	0.255
2	**0.011**	**0.044**	**0.008**	0.813	0.939	**0.006**	**0.019**	0.097	0.060
5	0.053	**0.001**	**<0.001**	0.878	0.642	**<0.001**	**0.023**	**<0.001**	**0.002**
10	**0.039**	**0.006**	**0.002**	0.589	0.965	**0.023**	0.051	**0.006**	**<0.001**
20	**0.010**	**0.007**	**<0.001**	0.343	0.936	**<0.001**	0.075	**0.010**	**<0.001**
30	**<0.001**	**0.021**	**<0.001**	0.227	0.793	**0.002**	**<0.001**	**0.026**	**<0.001**

Suppl. Table S4:

Changes in GC-MS based metabolite profiles in leaves of *trxf1*, *ntrc* and *trxf1 ntrc* Arabidopsis mutants compared to wild-type. Leaves were sampled at the end of the day. Results are means ± SD, *n* = 12. Values which are significantly different from wild type according to the student t-test (*P*<0.05) are indicated in bold (see also Figure 11A).

Metabolites	WT	*trx f1*	*P*-value	*ntrc*	P-value	*trxf1 ntrc*	*P*-value
Sugars							
Fructose	1.00 ± 0.57	**2.03 ± 0.69**	**0.001**	1.15 ± 0.37	0.445	0.83 ± 0.22	0.360
Glucose	1.00 ± 0.63	1.43 ± 0.63	0.109	**0.39 ± 0.08**	**0.006**	**0.45 ± 0.24**	**0.014**
Maltose	1.00 ± 0.26	1.03 ± 0.20	0.725	**1.65 ± 0.69**	**0.008**	**3.13 ± 1.34**	**<0.001**
Raffinose	1.00 ± 0.35	**1.93 ± 1.13**	**0.017**	**0.25 ± 0.07**	**<0.001**	**0.55 ± 0.64**	**0.045**
Ribose	1.00 ± 0.08	**1.15 ± 0.18**	**0.016**	**1.55 ± 0.51**	**0.003**	**2.64 ± 1.14**	**<0.001**
Sucrose	1.00 ± 0.07	**1.11 ± 0.10**	**0.004**	**0.86 ± 0.14**	**0.007**	**0.89 ± 0.07**	**0.001**
Trehalose	1.00 ± 0.49	**1.38 ± 0.23**	**0.028**	1.20 ± 0.44	0.304	**1.88 ± 0.75**	**0.003**
Phosphate ester							
Glycerol-3-phosphate	1.00 ± 0.27	1.14 ± 0.17	0.143	1.22 ± 0.47	0.174	**1.85 ± 1.02**	**0.016**
Phosphoenolpyruvate	1.00 ± 0.18	1.02 ± 0.20	0.805	1.35 ± 0.68	0.112	**1.85 ± 0.53**	**<0.001**
Organic acids							
Aconitate (cis)	1.00 ± 0.29	0.99 ± 0.32	0.956	0.84 ± 0.12	0.086	1.05 ± 0.36	0.711
Benzoate	1.00 ± 0.24	1.14 ± 0.32	0.257	1.33 ± 0.58	0.096	**1.61 ± 0.29**	**<0.001**
caffeate (cis)	1.00 ± 0.10	0.98 ± 0.10	0.593	1.09 ± 0.40	0.486	1.33 ± 0.93	0.247
caffeate (trans)	1.00 ± 0.36	1.03 ± 0.26	0.871	0.92 ± 0.20	0.594	1.10 ± 0.26	0.530
3-caffeoyl-quinate (cis)	1.00 ± 0.10	1.06 ± 0.16	0.306	**0.88 ± 0.15**	**0.033**	0.91 ± 0.18	0.138
3-caffeoyl-quinate (trans)	1.00 ± 0.22	1.23 ± 0.41	0.112	**0.59 ± 0.12**	**<0.001**	**0.74 ± 0.19**	**0.005**
Citrate	1.00 ± 0.19	1.09 ± 0.14	0.202	**0.69 ± 0.24**	**0.002**	**0.51 ± 0.38**	**0.001**

Fumarate	1.00 ± 0.17	1.05 ± 0.10	0.404	**0.80 ± 0.19**	**0.011**	**0.70 ± 0.22**	**0.001**
Galactonate	1.00 ± 0.12	0.95 ± 0.06	0.268	**0.88 ± 0.11**	**0.015**	**0.91 ± 0.06**	**0.029**
Glycerate	1.00 ± 0.04	**0.61 ± 0.07**	**<0.001**	**0.36 ± 0.18**	**<0.001**	**0.33 ± 0.44**	**<0.001**
Gulonate	1.00 ± 0.19	**1.28 ± 0.19**	**0.002**	**1.28 ± 0.38**	**0.033**	**1.42 ± 0.36**	**0.002**
Malate	1.00 ± 0.12	**1.22 ± 0.19**	**0.003**	1.00 ± 0.24	0.955	**0.69 ± 0.28**	**0.003**
Maleate	1.00 ± 0.51	0.85 ± 0.35	0.395	0.94 ± 0.36	0.726	1.51 ± 0.74	0.065
2-methyl-malate	1.00 ± 0.09	0.93 ± 0.17	0.206	**0.63 ± 0.18**	**<0.001**	**0.61 ± 0.21**	**<0.001**
2-oxo-glutarate	1.00 ± 0.18	0.92 ± 0.21	0.311	**0.66 ± 0.12**	**<0.001**	0.83 ± 0.36	0.281
Pyruvate	1.00 ± 0.35	0.79 ± 0.18	0.079	0.85 ± 0.23	0.225	1.02 ± 0.23	0.853
Shikimate	1.00 ± 0.08	1.11 ± 0.23	0.160	**0.52 ± 0.12**	**<0.001**	**0.51 ± 0.32**	**<0.001**
sinapate (cis)	1.00 ± 0.16	0.95 ± 0.16	0.485	0.97 ± 0.13	0.573	1.07 ± 0.19	0.370
sinapate (trans)	1.00 ± 0.22	0.91 ± 0.17	0.290	1.00 ± 0.22	0.987	**1.29 ± 0.40**	**0.040**
Succinate	1.00 ± 0.16	**0.80 ± 0.12**	**0.002**	**0.57 ± 0.15**	**<0.001**	**0.58 ± 0.35**	**0.002**
Threonate	1.00 ± 0.12	0.95 ± 0.18	0.416	**0.62 ± 0.05**	**<0.001**	**0.64 ± 0.14**	**<0.001**
Amino acids							
Alanine	1.00 ± 0.22	1.12 ± 0.37	0.357	1.07 ± 0.36	0.567	**1.36 ± 0.48**	**0.032**
Aspartate	1.00 ± 0.21	1.08 ± 0.33	0.496	1.24 ± 0.62	0.226	**1.75 ± 0.60**	**0.001**
Asparagine	1.00 ± 0.23	1.10 ± 0.17	0.368	1.21 ± 0.67	0.359	**1.95 ± 0.48**	**<0.001**
Glutamate	1.00 ± 0.27	1.03 ± 0.27	0.797	0.85 ± 0.26	0.179	1.05 ± 0.33	0.676
Glycine	1.00 ± 0.13	1.24 ± 0.38	0.055	**0.45 ± 0.17**	**<0.001**	**0.43 ± 0.31**	**<0.001**
4-hydroxy-proline (cis)	1.00 ± 0.28	0.77 ± 0.37	0.100	**0.38 ± 0.05**	**0.000**	0.85 ± 0.26	0.300
Isoleucine	1.00 ± 0.20	1.16 ± 0.30	0.136	1.48 ± 0.90	0.093	**2.30 ± 1.16**	**0.003**
Leucine	1.00 ± 0.172	**1.23 ± 0.19**	**0.007**	**1.40 ± 0.46**	**0.018**	**1.96 ± 1.00**	**0.007**
Methionine	1.00 ± 0.20	1.08 ± 0.31	0.470	1.12 ± 0.25	0.219	**1.37 ± 0.44**	**0.018**

Phenylalanine	1.00 ± 0.28	1.21 ± 0.25	0.073	3.16 ± 4.21	0.104	**6.74 ± 4.27**	**0.001**
Proline	1.00 ± 0.42	1.58 ± 0.90	0.059	2.30 ± 2.91	0.153	**7.16 ± 5.63**	**0.003**
Pyroglutamate	1.00 ± 0.33	1.22 ± 0.20	0.066	1.14 ± 0.38	0.356	**1.59 ± 0.51**	**0.003**
Serine	1.00 ± 0.36	0.75 ± 0.32	0.086	**0.50 ± 0.19**	**<0.001**	**0.57 ± 0.19**	**0.001**
Threonine	1.00 ± 0.21	1.06 ± 0.40	0.672	1.03 ± 0.39	0.845	1.19 ± 0.25	0.059
Valine	1.00 ± 0.15	1.12 ± 0.36	0.313	1.21 ± 0.71	0.339	**2.16 ± 1.16**	**0.005**
Sugar alcohols							
Erythritol	1.00 ± 0.14	**1.34 ± 0.20**	**0.003**	2.63 ± 2.82	0.072	**7.40 ± 3.30**	**<0.001**
Glycerol	1.00 ± 0.14	0.99 ± 0.19	0.918	1.09 ± 0.29	0.328	**1.41 ± 0.33**	**0.001**
Mannitol	1.00 ± 0.20	1.04 ± 0.30	0.738	2.91 ± 3.02	0.051	**8.07 ± 5.35**	**0.001**
myo-inositol	1.00 ± 0.16	1.19 ± 0.41	0.164	**0.44 ± 0.16**	**<0.001**	**0.42 ± 0.36**	**<0.001**
Sorbitol	1.00 ± 0.09	**0.87 ± 0.11**	**0.007**	1.04 ± 0.15	0.449	**1.24 ± 0.34**	**0.034**
Others							
4-amino-butanoate	1.00 ± 0.16	1.67 ± 1.31	0.105	1.17 ± 0.84	0.542	**4.92 ± 2.95**	**0.001**
Ascorbate	1.00 ± 0.52	**3.40 ± 2.32**	**0.004**	**4.22 ± 2.19**	**<0.001**	1.02 ± 0.60	0.947
Dehydroascorbate	1.00 ± 0.20	**1.44 ± 0.45**	**0.011**	**1.70 ± 0.64**	**0.003**	**1.76 ± 0.28**	**<0.001**
Ethanolamine	1.00 ± 0.26	**0.59 ± 0.14**	**<0.001**	**0.53 ± 0.17**	**<0.001**	1.00 ± 0.13	0.968
Phosphate	1.00 ± 0.13	1.02 ± 0.16	0.793	0.99 ± 0.18	0.847	1.07 ± 0.21	0.337
Putrescine	1.00 ± 0.29	1.06 ± 0.40	0.658	1.28 ± 0.52	0.124	**2.02 ± 1.10**	**0.009**
Spermidine	1.00 ± 0.67	1.13 ± 0.56	0.636	0.77 ± 0.47	0.355	0.74 ± 0.35	0.267
Uracil	1.00 ± 0.62	0.92 ± 0.48	0.763	1.24 ± 0.67	0.407	**3.42 ± 3.29**	**0.028**

Suppl. Table S5:

Changes in GC-MS based metabolite profiles in leaves of *trxf1*, *ntrc* and *trxf1 ntrc* Arabidopsis mutants compared to wild-type. Leaves were sampled at the end of the night. Results are means ± SD, *n* = 12. Values which are significantly different from wild type according to the student t-test (*P*<0.05) are indicated in bold (see also Figure 11B).

Metabolites	WT	*trx f1*	*P*-value	*ntrc*	*P*-value	*trxf1 ntrc*	*P*-value
Sugars							
Arabinose	1.00 ± 0.09	0.98 ± 0.08	0.549	0.95 ± 0.03	0.100	**0.70 ± 0.04**	**<0.001**
Fructose	1.00 ± 0.34	**0.38 ± 0.04**	**<0.001**	1.14 ± 0.46	0.397	1.14 ± 0.68	0.535
Galactose	1.00 ± 0.33	**0.56 ± 0.15**	**<0.001**	**0.31 ± 0.10**	**<0.001**	**0.39 ± 0.13**	**<0.001**
Glucose	1.00 ± 0.38	**0.35 ± 0.04**	**<0.001**	**0.20 ± 0.04**	**<0.001**	**0.34 ± 0.12**	**<0.001**
Glucose (beta-1,6-anhydro)	1.00 ± 0.19	**0.83 ± 0.16**	**0.025**	**0.80 ± 0.16**	**0.011**	1.15 ± 0.21	0.085
Maltose	1.00 ± 0.09	**0.73 ± 0.07**	**<0.001**	**0.51 ± 0.04**	**<0.001**	**0.19 ± 0.03**	**<0.001**
Mannose	1.00 ± 0.32	0.94 ± 0.19	0.615	0.81 ± 0.14	0.079	0.99 ± 0.17	0.905
Psicose	1.00 ± 0.05	**1.09 ± 0.06**	**<0.001**	0.99 ± 0.08	0.733	1.02 ± 0.04	0.230
Ribose	1.00 ± 0.17	1.04 ± 0.11	0.464	**1.17 ± 0.11**	**0.011**	**2.71 ± 0.45**	**<0.001**
Sucrose	1.00 ± 0.03	**0.82 ± 0.09**	**<0.001**	**0.53 ± 0.04**	**<0.001**	**0.46 ± 0.04**	**<0.001**
Trehalose	1.00 ± 0.28	1.11 ± 0.19	0.283	0.86 ± 0.21	0.168	1.08 ± 0.14	0.386
Xylose	1.00 ± 0.18	0.88 ± 0.10	0.055	**0.84 ± 0.11**	**0.014**	1.11 ± 0.17	0.124
Organic acids							
Citrate	1.00 ± 0.26	**1.53 ± 0.23**	**<0.001**	0.99 ± 0.25	0.924	**1.23 ± 0.26**	**0.036**
Fumarate	1.00 ± 0.20	0.92 ± 0.11	0.256	0.89 ± 0.09	0.107	**0.59 ± 0.06**	**<0.001**
Glycerate	1.00 ± 0.13	**1.13 ± 0.09**	**0.011**	0.90 ± 0.18	0.120	**0.70 ± 0.09**	**<0.001**
Hexadecanoate	1.00 ± 0.55	**0.58 ± 0.22**	**0.026**	**0.54 ± 0.17**	**0.016**	**0.57 ± 0.18**	**0.022**

Malate	1.00 ± 0.22	1.06 ± 0.12	0.437	1.12 ± 0.25	0.216	**1.54 ± 0.15**	**<0.001**
Maleate	1.00 ± 0.14	1.00 ± 0.16	0.985	1.10 ± 0.20	0.167	**1.87 ± 0.22**	**<0.001**
Octadecanoate	1.00 ± 0.62	0.69 ± 0.29	0.134	0.65 ± 0.23	0.088	0.70 ± 0.25	0.134
Pyroglutamate	1.00 ± 0.19	1.05 ± 0.13	0.435	**1.66 ± 0.14**	**<0.001**	**2.04 ± 0.14**	**<0.001**
Pyruvate	1.00 ± 0.29	**0.75 ± 0.18**	**0.018**	**0.68 ± 0.18**	**0.003**	**0.71 ± 0.19**	**0.007**
Shikimate	1.00 ± 0.07	**1.17 ± 0.11**	**<0.001**	**0.87 ± 0.09**	**<0.001**	**0.69 ± 0.07**	**<0.001**
Sinapate (cis)	1.00 ± 0.11	1.00 ± 0.16	0.991	1.00 ± 0.06	0.993	**1.45 ± 0.10**	**<0.001**
Sinapate (trans)	1.00 ± 0.14	**1.11 ± 0.09**	**0.028**	**1.14 ± 0.11**	**0.015**	**1.68 ± 0.14**	**<0.001**
Succinate	1.00 ± 0.14	**0.82 ± 0.10**	**0.002**	**0.86 ± 0.12**	**0.018**	**0.59 ± 0.06**	**<0.001**
Threonate	1.00 ± 0.11	**1.24 ± 0.12**	**<0.001**	**1.42 ± 0.45**	**0.009**	0.94 ± 0.15	0.310
Amino acids							
Alanine	1.00 ± 0.13	**1.25 ± 0.11**	**<0.001**	**1.64 ± 0.15**	**<0.001**	**3.03 ± 0.19**	**<0.001**
Arginine	1.00 ± 0.25	1.22 ± 0.29	0.057	**1.27 ± 0.32**	**0.031**	**7.53 ± 3.62**	**<0.001**
Asparagine	1.00 ± 0.43	1.02 ± 0.28	0.881	**2.41 ± 1.65**	**0.014**	**43.70 ± 9.51**	**<0.001**
Aspartate	1.00 ± 0.48	0.93 ± 0.36	0.686	0.77 ± 0.51	0.272	1.14 ± 0.62	0.543
Glutamate	1.00 ± 0.30	**1.40 ± 0.18**	**<0.001**	**1.48 ± 0.24**	**<0.001**	**1.88 ± 0.12**	**<0.001**
Glycine	1.00 ± 0.43	**0.67 ± 0.13**	**0.027**	**0.42 ± 0.06**	**<0.001**	0.77 ± 0.26	0.134
Isoleucine	1.00 ± 0.15	1.04 ± 0.29	0.665	1.15 ± 0.30	0.141	**3.98 ± 0.54**	**<0.001**
Leucine	1.00 ± 0.16	0.99 ± 0.40	0.952	1.05 ± 0.51	0.731	**3.28 ± 0.52**	**<0.001**
Lysine	1.00 ± 0.25	1.14 ± 0.28	0.215	**1.52 ± 0.76**	**0.034**	**10.21 ± 3.01**	**<0.001**
Phenylalanine	1.00 ± 0.33	**1.36 ± 0.37**	**0.019**	0.82 ± 0.22	0.135	**10.28 ± 1.84**	**<0.001**
Proline	1.00 ± 0.44	0.80 ± 0.33	0.225	**0.49 ± 0.18**	**0.002**	**2.36 ± 0.38**	**<0.001**
Serine	1.00 ± 0.27	1.05 ± 0.16	0.547	**1.25 ± 0.14**	**0.010**	**2.33 ± 0.28**	**<0.001**
Threonine	1.00 ± 0.20	1.07 ± 0.08	0.314	1.13 ± 0.14	0.087	**1.99 ± 0.16**	**<0.001**

Valine	1.00 ± 0.19	1.04 ± 0.17	0.578	1.13 ± 0.22	0.124	**2.59 ± 0.24**	**<0.001**
Sugar alcohols							
Erythritol	1.00 ± 0.19	1.12 ± 0.07	0.051	**1.63 ± 0.23**	**<0.001**	**5.96 ± 0.77**	**<0.001**
Glycerol	1.00 ± 0.13	1.12 ± 0.18	0.081	0.99 ± 0.14	0.870	**1.33 ± 0.16**	**<0.001**
Inositol (myo)	1.00 ± 0.11	1.00 ± 0.07	0.985	**0.47 ± 0.06**	**<0.001**	**0.19 ± 0.03**	**<0.001**
Mannitol	1.00 ± 0.64	0.74 ± 0.19	0.200	**2.90 ± 0.90**	**<0.001**	**18.26 ± 6.04**	**<0.001**
Sorbitol	1.00 ± 0.07	**0.90 ± 0.06**	**0.001**	0.96 ± 0.09	0.192	**1.37 ± 0.07**	**<0.001**
Others							
Ascorbate	1.00 ± 0.68	0.66 ± 0.25	0.126	0.87 ± 0.81	0.680	1.03 ± 0.32	0.895
Dehydroascorbate	1.00 ± 0.25	0.86 ± 0.11	0.087	0.82 ± 0.23	0.083	1.14 ± 0.29	0.228
Ethanolamine	1.00 ± 0.34	0.85 ± 0.12	0.163	1.02 ± 0.17	0.888	1.34 ± 0.48	0.058
Phosphate	1.00 ± 0.15	1.01 ± 0.14	0.865	**0.67 ± 0.14**	**<0.001**	**1.88 ± 0.14**	**<0.001**
Putrescine	1.00 ± 0.36	1.06 ± 0.27	0.664	**1.36 ± 0.48**	**0.048**	**3.65 ± 0.42**	**<0.001**
Spermidine	1.00 ± 0.54	1.34 ± 0.52	0.135	**2.62 ± 0.99**	**<0.001**	**2.44 ± 1.81**	**0.021**
Uracil	1.00 ± 0.19	**0.74 ± 0.18**	**0.002**	**0.80 ± 0.16**	**0.011**	**4.40 ± 0.56**	**<0.001**

Suppl. Table S6:

Changes in the levels of phosphorylated intermediates and starch in leaves of *trxf1*, *ntrc* and *trxf1 ntrc Arabidopsis* mutants compared to wild-type, based on spectrophotometric measurements. Leaves were sampled at the end of the day. Results are normalized to wild-type level and represent means ± SE, *n* = 8-30 (wild-type) or 4-15 (mutants). Values which are significantly different from wild-type according to the student t-test (*P*<0.05) are indicated in bold (see also Figure 11A).

Metabolites	WT	*trxf1*	*P-value*	*ntrc*	*P-value*	*trxf1 ntrc*	*P-value*
Dihydroxyacetone phosphate	1.00 ± 0.03	**1.22 ± 0.06**	**0.001**	**1.69 ± 0.10**	**<0.001**	0.99 ± 0.14	0.926
Fructose 1,6-bisphosphate	1.00 ± 0.04	**1.50 ± 0.08**	**<0.001**	**2.25 ± 0.14**	**<0.001**	**1.76 ± 0.20**	**0.002**
Fructose 6-phosphate	1.00 ± 0.03	**1.29 ± 0.07**	**0.001**	**1.31 ± 0.07**	**<0.001**	**0.73 ± 0.05**	**<0.001**
Glucose 1-phosphate	1.00 ± 0.09	0.88 ± 0.12	0.432	1.54 ± 0.15	**0.003**	0.82 ± 0.16	0.282
Glucose 6-phosphate	1.00 ± 0.02	1.00 ± 0.03	0.997	1.06 ± 0.05	0.207	**0.73 ± 0.04**	**<0.001**
Glyceraldehyde 3-phosphate	1.00 ± 0.04	**1.25 ± 0.09**	**0.006**	**1.68 ± 0.11**	**<0.001**	0.92 ± 0.09	0.389
3-Phosphoglycerate	1.00 ± 0.04	1.10 ± 0.06	0.139	**0.66 ± 0.04**	**<0.001**	**0.26 ± 0.02**	**<0.001**
Starch	1.00 ± 0.04	**0.79 ± 0.02**	**0.009**	**0.66 ± 0.04**	**<0.001**	**0.26 ± 0.01**	**<0.001**

Suppl. Table S7:

Changes in the levels of phosphorylated intermediates and starch in leaves of *trxf1*, *ntrc* and *trxf1 ntrc Arabidopsis* mutants compared to wild-type, based on spectrophotometric measurements. Leaves were sampled at the end of the night. Results are normalized to wild-type level and represent means ± SE, *n* = 8-30 (wild-type) or 4-15 (mutants). Values which are significantly different from wild-type according to the student t-test (*P*<0.05) are indicated in bold (see also Figure 11B). n.d. = not detectable.

Metabolites	WT	*trxf1*	*P*-value	*ntrc*	*P*-value	*trxf1 ntrc*	*P-value*
Dihydroxyacetone phosphate	1.00 ± 0.03	0.96 ± 0.08	0.608	**0.73 ± 0.03**	**<0.001**	**0.65 ± 0.07**	**<0.001**
Fructose 1,6-bisphosphate	n.d.	n.d.		n.d.		n.d.	
Fructose 6-phosphate	1.00 ± 0.07	0.88 ± 0.09	0.322	1.14 ± 0.21	0.549	**0.36 ± 0.05**	**<0.001**
Glucose 1-phosphate	1.00 ± 0.11	1.18 ± 0.16	0.364	1.86 ± 0.38	0.053	**0.62 ± 0.12**	**0.042**
Glucose 6-phosphate	1.00 ± 0.03	0.92 ± 0.04	0.106	**0.73 ± 0.03**	**<0.001**	**0.38 ± 0.04**	**<0.001**
Glyceraldehyde 3-phosphate	n.d.	n.d.		n.d.		n.d.	
3-Phosphoglycerate	1.00 ± 0.05	1.03 ± 0.08	0.771	**0.80 ± 0.07**	**0.026**	**0.51 ± 0.06**	**<0.001**
Starch	1.00 ± 0.20	**0.36 ± 0.05**	**0.014**	**0.26 ± 0.02**	**0.007**	**0.09 ± 0.01**	**0.002**